Green Chemistry

ROYAL SOCIETY OF CHEMISTRY

TUTORIAL REVIEW

View Article Online
View Journal

Cite this: DOI: 10.1039/d5gc02486b

Advances in catalytic conversion of ethanol to higher alcohols as liquid fuels and aviation fuel precursors

Rongqi Lei,[a] Zetong Chen,[a] Quanzhou Xu,[a] Nan Wang,[a] Yanlin Qin, [a,b,c] Tiejun Wang, [a,b,c] Xuliang Lin *[a,b,c] and Xueqin Qiu *[a,b,c]

Received 19th May 2025,
Accepted 21st July 2025

DOI: 10.1039/d5gc02486b

rsc.li/greenchem

As a renewable green energy source, the catalytic upgrading of ethanol to higher alcohols (C_{4+}) represents a critical pathway to overcome its inherent fuel limitations. C_8–C_{16} isomer groups within higher alcohols are utilized as pivotal intermediates in synthesizing sustainable aviation fuels (SAFs) *via* hydrodeoxygenation—a catalytic process critical for meeting globally mandated emission reduction targets in the aviation sector. This review comprehensively analyzes reaction mechanisms and catalyst design strategies for ethanol valorization, emphasizing the pivotal roles of acid-base synergy, metal-support electronic interactions, and dynamic intermediate regulation. While non-precious metal catalysts demonstrate scalable potential, challenges persist in aqueous-phase stability and long-chain selectivity. Future breakthroughs demand the integration of *in situ* characterization and multiscale simulations to engineer robust, water-tolerant catalytic systems, ultimately advancing the high-value transformation of bioethanol into drop-in biofuels and SAF precursors.

Green foundation

1. This review highlights catalytic innovations enabling ethanol upgrading to higher alcohols (C_{4+}) *via* non-precious metal catalysts, biomass-derived carbon supports. Acid-base synergy and metal-support interactions enhance selectivity and stability, while hydrodeoxygenation converts C_8–C_{16} alcohols into sustainable aviation fuels (SAFs), aligning with circular economy principles.
2. Ethanol-derived higher alcohols address fossil fuel limitations by offering renewable, energy-dense alternatives compatible with existing infrastructure. Their role as SAF precursors supports global emission reduction mandates in aviation, while bioethanol utilization promotes agricultural and marine biomass valorization, bridging energy security and environmental sustainability.
3. Future breakthroughs demand water-tolerant catalysts and mechanistic insights *via in situ* characterization. This review guides the design of robust systems for scalable biofuel production, accelerating the transition to carbon-neutral energy. By linking catalyst engineering with industrial needs, it fosters interdisciplinary innovation in green chemistry and sustainable fuel synthesis.

1 Introduction

The overexploitation of fossil resources has precipitated-unprecedented carbon emissions and environmental degradation, driving global urgency to address energy security and sustainability.[1–3] Amidst dwindling reserves and volatile energy prices, the demand for green and efficient alternatives has intensified to meet societal and economic needs.[4–8]

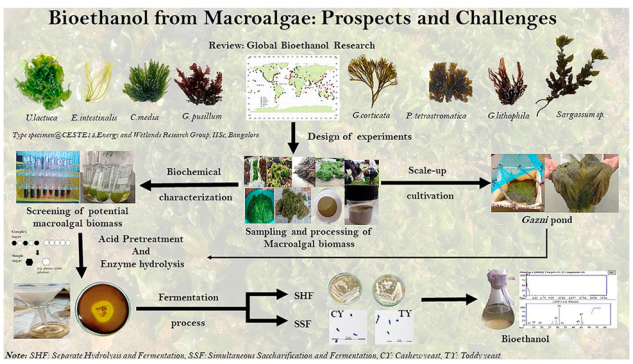

Fig. 1 Bioethanol derived from macroalgae species underscores marine biomass as a sustainable, renewable source for ethanol production,[39] copyright 2020, Elsevier.

[a]*Guangdong Provincial Key Laboratory of Plant Resources Biorefinery, School of Chemical Engineering and Light Industry, Guangdong University of Technology, Guangzhou 510006, China. E-mail: xllin@gdut.edu.cn, cexqqiu@scut.edu.cn*
[b]*Guangdong Provincial Laboratory of Chemistry and Fine Chemical Engineering Jieyang Center, Jieyang 515200, China*
[c]*Guangdong Basic Research Center of Excellence for Ecological Security and Green Development, Guangdong University of Technology, Guangzhou 510006, China*

Table 1 Comparative analysis of the physicochemical properties of lower alcohols, higher alcohols, and diesel fuel

Fuel	Methanol	Ethanol	Butanol	Hexanol	Octanol	Vegetable alcohol	Diesel
Molecular formula	CH_3OH	C_2H_5OH	C_4H_9OH	$C_6H_{13}OH$	$C_8H_{17}OH$	$C_{20}H_{39}OH$	C_xH_y
Cetane number	5	8	17	23	39	45.9	52
Autoignition temperature (°C)	463	420	345	285	270	—	254–300
Lower heating value (MJ kg^{-1})	19.58	26.83	33.09	39.10	52.94	43.6	42.49
Heat of vaporization (kJ kg^{-1})	1162.64	918.42	581.4	486	—	—	270–375
Vapor pressure (mmHg)	127	55	7	1	0.08	—	0.4
Boiling point (°C)	64.7	78.3	117.5	157	195	204	180–360
Flash point (°C)	11–12	17	35–37	59	81	—	>55

Bioethanol, a renewable feedstock derived from sugar, starch, macroalgae and lignocellulosic biomass (Fig. 1), emerges as a strategic candidate for fossil fuel replacement due to its abundance and scalability, particularly in leading producers like the United States and Brazil.[8–11] However, its hygroscopicity, corrosivity, and low energy density limit direct applications in existing fuel infrastructure.[12–14] In contrast, higher carbon alcohols (C_{4+}), characterized by superior hydrophobicity, reduced corrosivity, and energy densities comparable to diesel, present a transformative solution.[15,16] The physicochemical properties of representative higher alcohols compared with lower alcohols and diesel fuel are presented in Table 1.[17–19] These alcohols not only align with existing logistics but also serve as precursors for sustainable aviation fuels (SAFs) after hydrodeoxygenation.[20–22] Catalytic conversion technologies are pivotal for upgrading ethanol into value-added fuels, yet challenges persist in selectivity, catalyst deactivation, and recyclability.[23] Notably, biological fermentation (*e.g.*, acetone–butanol–ethanol [ABE] pathway) has historically enabled higher alcohols production,[24,25] but faces limitations in product titer and substrate versatility.[26] Concurrently, CO_2 valorization to higher alcohols *via* thermocatalytic or electrocatalytic hydrogenation has emerged as a complementary sustainable pathway,[27–33] leveraging similar catalytic principles (*e.g.*, metal-oxide interfaces, C–C coupling) to ethanol transformation.[34–38]

Over the past decade, bio-aviation fuels have garnered significant scientific attention. Seminal reviews have systematically mapped the field's technological landscape and future trajectories,[40–49] establishing biomass as a viable sustainable feedstock while underscoring catalytic conversion as the critical pathway to bio-jet fuels.[45,50] Within this framework, synergistic bio-chemo-catalytic strategies emerge as pivotal solutions for enhancing efficiency and cost-effectiveness,[49] particularly for converting bio-ethanol platform molecules to aviation kerosene.[47] Building on these foundations, this review critically examines recent advances in both homogeneous and heterogeneous catalytic systems, with a dedicated focus on their ethanol conversion efficiency and selectivity. Crucially, we identify key constraints in current methodologies and propose targeted innovations to advance catalytic systems for industrial-scale sustainable aviation fuel (SAF) synthesis.

2 Mechanisms of higher alcohol production

2.1 Carbonyl synthesis *via* hydroformylation

Hydroformylation stands as a cornerstone industrial method for higher alcohol synthesis, distinguished by its high atom economy and alignment with green chemistry principles. The reaction mechanism involves sequential adsorption/activation of CO and H_2 on catalytic surfaces, followed by olefin insertion and hydrogenation to yield aldehydes and alcohols.[51] Catalyst innovation drives this field, with current research focusing

Rongqi Lei

Rongqi Lei is currently pursuing a master's degree in Chemical Engineering at Guangdong University of Technology under the supervision of Professor Xuliang Lin. His research focuses on the design and preparation of catalysts, as well as the catalytic performance and mechanistic study of higher alcohol synthesis via bioethanol coupling reactions.

Zetong Chen

Zetong Chen is currently pursuing a master's degree in Chemical Engineering at Guangdong University of Technology under the supervision of Professor Xuliang Lin. His research focuses on the design and preparation of lignin-derived carbon-based catalysts, as well as comprehensive studies on their catalytic performance, reaction mechanisms, and potential industrial applications in the coupling conversion of bioethanol to higher alcohols.

on:[52–61] noble metal systems (Rh, Mo): exhibiting superior activity under mild conditions with exceptional linear product selectivity. Rhodium-based catalysts, despite their prohibitive cost, remain unmatched in selectivity for straight-chain alcohols;[62,63] non-noble alternatives (Cu, Co): emerging as cost-effective candidates requiring further optimization in activity and stability.

2.2 Ethanol condensation pathways

2.2.1 Direct dimerization mechanism. The coupling of ethanol to produce higher alcohols mainly proceeds *via* two reaction pathways. Yang *et al.*[64] proposed a direct condensation route involving two ethanol molecules, as shown in Fig. 2a. Under the action of a catalyst, ethanol undergoes direct dehydration condensation to form *n*-butanol with the release of a water molecule. This pathway features a relatively simple mechanism; however, it often suffers from low selectivity and high activation energy, which limits its efficiency in practical applications.

2.2.2 Guerbet coupling mechanism. The second pathway is the classical Guerbet reaction mechanism (Fig. 2b), which involves a series of indirect and stepwise transformations. Initially, ethanol is dehydrogenated to form acetaldehyde. Under basic conditions, two acetaldehyde molecules undergo aldol condensation to generate 3-hydroxybutanal, which subsequently dehydrates to form crotonaldehyde. Crotonaldehyde can then be partially hydrogenated to *n*-butanal in a hydrogen atmosphere, and further complete hydrogenation yields *n*-butanol. It is worth noting that the resulting *n*-butanal can undergo self-aldol condensation or cross-condensation with acetaldehyde, leading to the formation of branched aldehydes, which can then be hydrogenated to the corresponding higher alcohols. *n*-Butanal is merely one example—hexanal may also participate in self- or cross-condensation reactions with acetaldehyde, *n*-butanal, or itself. As the carbon chain length increases, the diversity of possible intermediates also increases.

It is important to emphasize that Gu *et al.*[65] pointed out that the *n*-butanal generated in this process primarily originates from the aforementioned condensation-hydrogenation pathway intermediates, rather than from the reverse dehydrogenation of *n*-butanol, as the latter requires a significantly higher activation energy.[66] Therefore, effective control over the dehydrogenation-condensation-hydrogenation sequence is critical for promoting carbon chain growth while suppressing over-hydrogenation and undesirable cleavage reactions.

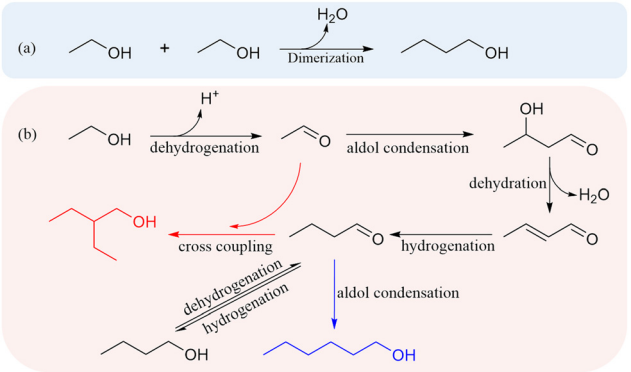

Fig. 2 Schematic illustration of the reaction pathways for higher alcohol synthesis *via* ethanol coupling: (a) *n*-butanol formation through direct dehydration condensation of ethanol; (b) Guerbet reaction mechanism starting from ethanol, involving multiple reaction pathways and intermediates (using *n*-butanal as an example).

3 Catalytic systems for bioethanol upgrading to higher alcohols

3.1 Homogeneous catalysts

Catalytically homogeneous frameworks enable atomic-scale engineering of reactive sites, facilitating ethanol transformation at low operational intensities while maintaining exceptional kinetic performance. This uniform catalytic environment guarantees complete exposure of active centers to substrates, thereby optimizing catalytic efficiency—a pivotal feature in upgrading bioethanol.

Yanlin Qin

Qin Yanlin, Professor of Guangdong University of Technology, Deputy Director of Science and Technology Department. Committed to the efficient utilization of renewable resources such as lignocellulose conversion, carbon fiber materials, biomass carbon catalysis and technical lignin functionalization and the transformation of low-carbon industries. Deputy editor-in-chief of Biochar.X, young editorial board of Rare Metals and Carbon Research.

Tiejun Wang

Tiejun Wang, received his Ph.D. from University of Science and Technology of China, is currently a professor and doctoral supervisor of Guangdong University of Technology, a member of the Biomass Energy Professional Committee of China Renewable Energy Society, and the head of the Danish "C3B0 Biofuel Project". His main research interests are bioenergy, energy and environmental catalysis, fuel chemistry and low-carbon technology.

3.1.1 Iridium-based catalysts. Iridium complexes demonstrate exceptional versatility in ethanol upgrading. Koda *et al.*[67] pioneered the use of [Ir(acac)(cod)] with sodium ethoxide as a base, achieving 41.0% ethanol conversion and 51.0% 1-butanol selectivity at 120 °C (15 h). To address aqueous-phase limitations, Xu *et al.*[68] engineered a water-stable $Ir(OAc)_3$/L10 (disodium phenanthroline disulfonate) system, attaining 54.0% conversion and 91.0% higher alcohol selectivity at 150 °C (12 h), with retained activity over three cycles.

A breakthrough in selectivity control was achieved by Chakraborty *et al.*,[69] who designed a sterically congested Ir-[Tp′Ni(μ-OH)]$_2$ catalyst (1 : 25 ratio) for tandem Guerbet coupling. This system delivered 37.0% ethanol conversion with >99.0% 1-butanol selectivity at 150 °C (24 h), where the spatial dense structure of nickel and copper hydroxide promoted the key aldehyde coupling reaction of acetaldehyde, and only C_4 coupling product, crotonaldehyde, was produced. The iridium center facilitated ethanol dehydrogenation at reduced temperatures, while the bulky metal hydroxide framework directed selective C_4 aldol coupling—a rare demonstration of steric control in homogeneous catalysis.

3.1.2 Ruthenium-based catalysts. Ruthenium catalysts exhibit comparable catalytic efficacy in ethanol coupling reactions. Dowson *et al.*[70] demonstrated the potential of [RuCl(η^6-*p*-cymene)]Cl for bioethanol upgrading, achieving 93.6% 1-butanol selectivity with 22.1% ethanol conversion at 150 °C within 4 h. Mechanistic studies revealed that uncontrolled aldol condensation of acetaldehyde intermediates underpinned the high selectivity. To address the modest conversion, Wingad *et al.*[71] from the same team redesigned the catalyst by incorporating hybrid phosphine-amine ligands into [$RuCl_2$(η^6-*p*-cymene)]$_2$. This modification boosted ethanol conversion to 31.4% while maintaining 92.7% selectivity, attributed to ligand-assisted proton transfer mechanisms.

Further optimizing reaction conditions, DiBenedetto *et al.*[72] explored the impact of water-ethanol ratios using [Ru(bipyOH)]. At an optimal 84 : 16 H_2O : EtOH ratio and 80 °C, the system delivered 49.1% ethanol conversion with 57.0% 1-butanol selectivity over 18 h. Deviating to a 91 : 9 ratio reduced performance but enabled trace amounts of long-chain alcohols, highlighting solvent composition as a critical selectivity lever. Tseng *et al.*[73] advanced reaction kinetics with an N,N,N-Ru(II) pincer complex, achieving 53.0% conversion and 80.0% selectivity in merely 2 h at 150 °C with ultralow catalyst loading (0.1 mol%), demonstrating unprecedented time efficiency.

Pushing beyond C_4 alcohols, Xie *et al.*[74] engineered a ruthenium pincer catalyst for cascade coupling under N_2 atmosphere. Extended reaction duration (40 h at 150 °C) yielded 73.4% ethanol conversion with >99.0% selectivity toward C_4–C_8 alcohols, showcasing the system's capacity for long-chain alcohol synthesis. Farris *et al.*[75] decoupled catalyst stability challenges in Ru(R-bpi)$(PPh_3)_n$Cl pre-catalysts. By introducing 5-methyl substitution on bpi ligands, they suppressed hydrogenolytic decomposition—the primary deactivation pathway—enhancing both activity and stability. Ru-2 outperformed Ru-1 with 65% *versus* 58% yield within 2 h, validating strategic ligand modifications to protect imine bonds as a viable design strategy. The mechanism of action of the rhodium-based catalyst is shown in Fig. 3.

3.1.3 Manganese-based catalysts. While iridium- and ruthenium-based homogeneous catalysts exhibit exceptional performance, their reliance on precious metals poses significant cost barriers for industrial-scale applications. Addressing this challenge, Fu *et al.*[76] pioneered the first homogeneous non-precious metal catalytic system using manganese porphyrin complexes for ethanol upgrading *via* the Guerbet reaction. The catalytic cycle begins with the pre-catalyst [Mn]-1a reacting with sodium ethoxide to form the active species [Mn]-

Xuliang Lin

Xuliang Lin, Professor at Guangdong University of Technology, and Assistant Dean of the Faculty of Light Industry and Chemical Engineering. His primary research focuses on the fundamental research and application of lignin carbon-based catalytic materials, especially in the fields of thermocatalysis, photocatalysis and electrocatalysis. Prof. Lin has authored or co-authored over 110 articles in prestigious journals with a Google Scholar h-index of 35.

Xueqing Qiu

Xueqing Qiu, is a professor leading the research group of high utilization of lignocellulose at Guangdong University of Technology (GDUT). Prof. Qiu serves as the president of GDUT and is recognized as a fellow of the Canadian Academy of Engineering. He serves as the vice chairman of the Guangdong Provincial Association for Science and Technology, fellow of the Global Chinese Scholars Association for Chemical Engineering, and executive director of the Guangdong Provincial Chemical Society. He is renowned for his expertise in lignocellulose biorefinery, particularly lignin into green fine chemicals and advanced materials.

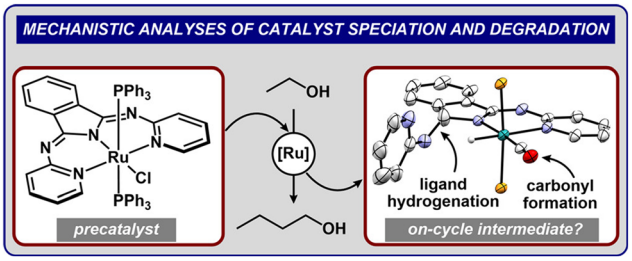

Fig. 3 The mechanism of action of rhodium-based catalysts.[75] copyright 2024, American Chemical Society.

1d, which subsequently undergoes β-hydride elimination to generate a manganese hydride intermediate ([Mn]-1e) while releasing acetaldehyde. Under alkaline conditions, the acetaldehyde undergoes aldol condensation to produce crotyl alcohol, which is then reduced by the hydride species to yield 1-butanol, regenerating the catalyst through ethanolysis of the resulting amide complex ([Mn]-1c). This system demonstrated remarkable longevity, maintaining 11.2% ethanol conversion and 92.0% 1-butanol selectivity over 168 hours at 160 °C.

Kulkarni *et al.*[77] further advanced manganese-catalyzed systems by optimizing reaction parameters and ligand design. Using $[HN(CH_2CH_2PPh_2)_2]Mn(CO)_2Br$ with NaOEt at 150 °C for 24 hours, they achieved 72.0% ethanol conversion and 69.5% higher alcohols selectivity. Their work identified critical structure-activity relationships: the synergistic interaction between phosphine substituents and the metal-ligand N–H functionality enhanced catalytic activity, while water generated during the reaction emerged as a primary deactivation pathway. To mitigate these limitations, Roca Jungfer *et al.*[78] introduced a bimetallic Mn(I)–Ru(II) system, which exhibited a striking synergistic effect in the Guerbet reaction. Integrated catalytic architectures enhance both reaction rate and spatial efficiency, simultaneously boosting process throughput and minimizing alkaline reagent requirements. Homogeneous catalysts are bonded to metals through ligands.

Homogeneous catalysts excel in molecular-level control over ethanol dehydrogenation and C–C coupling, providing invaluable mechanistic insights. However, their practical deployment remains constrained by three interrelated challenges: (i) the high cost of noble metals, (ii) environmental concerns associated with organic solvents, and (iii) limited recyclability under prolonged operation. The inherent scarcity of precious metals such as iridium and ruthenium within the Earth's crust dictates their high cost, significantly constraining their large-scale industrial deployment. Iridium ranks among the least abundant elements in the Earth's crust, with an average mass fraction of 0.001 ppm in crustal rocks.[79] In stark contrast, manganese is an abundant metallic element within the Earth's crust, exhibiting widespread distribution across rocks and sediments.[80,81] For instance, elevated manganese concentrations, ranging from 739 to 2260 ppm, are observed in suspended sediments of the Mississippi River and deposits within the Gulf of Mexico.[82] Furthermore, global manganese ore supply demonstrates high geopolitical concentration, with extraction costs estimated at less than one-thousandth of those for iridium.[83] Critically, enriched precious metals can also be extracted from marine ferromanganese crusts.[84,85] This profound price differential inevitably exerts a decisive influence on industrial material selection.

Nevertheless, the widespread industrial adoption of non-precious manganese-based catalysts remains impractical. This limitation stems primarily from manganese's complex biological role. While an essential metal serving as a cofactor for metalloenzymes critical in regulating the glutamate/glutamine cycle and other oxidative stress pathways, manganese poses significant neurotoxic risks upon excessive exposure. Such overexposure typically arises from ingesting inadequately treated well water or inhaling manganese-laden industrial byproducts. Manganese toxicity disrupts dopaminergic neurotransmission, precipitating a Parkinsonian syndrome termed manganism.[86] Conversely, precious metals like iridium and ruthenium hold promise as metalloantibiotics for targeted cancer therapy within biomedicine.[87,88] However, their potential cytotoxicity towards healthy human cells necessitates thorough further evaluation.[89,90] Ultimately, the major barriers impeding the large-scale industrial application of metal complexes, including those based on precious metals, are twofold: the environmental hazards associated with heavy metal leaching and the inherent challenge of recovering homogeneous catalysts from reaction systems, thus creating significant economic and sustainability hurdles. These limitations have driven a paradigm shift toward heterogeneous systems that leverage support confinement effects and metal-carrier interactions to reconcile high activity with cost-effective separations and enhanced stability—a transition critical for scalable biofuel production.

3.2 Heterogeneous catalysts

Heterogeneous catalysts are industrially favored for ethanol upgrading due to their reusability, facile separation, and scalability. These systems operate through interfacial reactions between solid catalysts and liquid reactants, with major categories including zeolites, magnesium-aluminum mixed metal oxides, hydroxyapatite (HAP), and carbon-based materials.

3.2.1 Zeolites catalysts. Zeolites leverage intrinsic acid-base sites to drive ethanol condensation. Pioneering work by Yang *et al.*[64] demonstrated alkali cation-exchanged zeolites (*e.g.*, Rb-LiX) catalyze ethanol-to-1-butanol conversion *via* β-C–H activation rather than classical aldol pathways. At 420 °C with a contact time ($W/F_{ethanol}$) of 5.6 (h g) mol^{-1}, their system achieved 20.8% ethanol conversion and 40.9% 1-butanol selectivity. Kots *et al.*[91] advanced this paradigm by designing Pd-doped Zr-BEA zeolites with bifunctional active sites. For example, metal sites such as Pd nanoparticles facilitate ethanol dehydrogenation to acetaldehyde. Acid-base sites enable sequential aldol condensation and hydrogenation to yield 1-butanol. Hydrogen atmosphere effectively mitigates carbonate/acetate deposition on metallic interfaces through surface passivation, whereas water molecules preferentially

occupying acidic domains prevent parasitic reactions. Unlike physically blended acid-base components, catalysts with colocalized active sites enhance synergistic effects between dehydrogenation and condensation pathways. In a groundbreaking design by Lu *et al.*,[92] their bm-BEA@oxide composite catalyst features adjacent acid-base interfaces (Fig. 4a). This architecture concurrently accelerates dehydrogenation and condensation rates, exhibiting 24.0% ethanol conversion and 81.0% butanol selectivity under closely integrated dual-site conditions -an 8-fold enhancement over physical mixtures of bm-BEA and Mg–Al oxides (Fig. 4b and e). The catalyst further demonstrates superior performance against redox-containing catalysts and conventional acid-base systems (Fig. 4c). Mechanistic investigations employing kinetic analysis, *in situ* FTIR spectroscopy, and DFT calculations confirm that the acetaldehyde intermediate, generated *via* ethanol dehydrogenation, undergoes C–C coupling to form butanol (Fig. 4d and f). The proximal dual sites drive the high butanol yield by synergistically promoting both dehydrogenation and the subsequent aldol condensation (Fig. 4g).

Building on zeolite design principles, Liu *et al.*[94] engineered a bifunctional Pt–Y/β catalyst *via* solid-state ion exchange and impregnation. Yttrium moieties incorporate into zeolitic matrices *via* silanol bonding at structural imperfections, whereas platinum nanoclusters deposit uniformly across external surfaces. This spatial organization enabled synergistic catalysis: Pt sites drove ethanol dehydrogenation and subsequent crotonaldehyde hydrogenation, while Y sites mediated acetaldehyde condensation. The optimized architecture achieved 34.0% ethanol conversion with 68.0% 1-butanol selectivity,

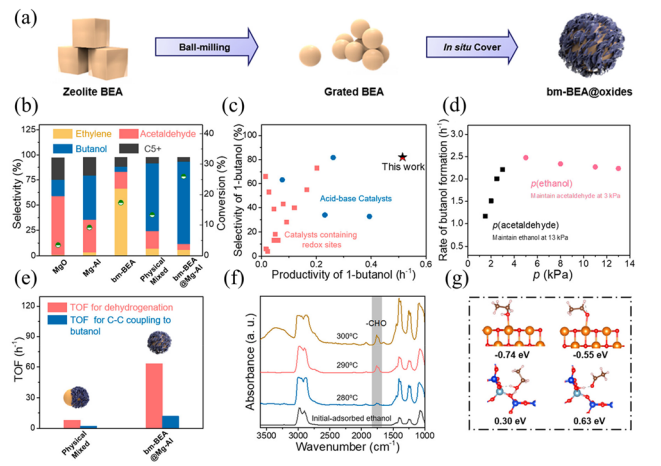

Fig. 4 (a) Schematic illustration of the synthetic process of the acid–base mixed catalysts. (b) 1-Butanol selectivity and apparent mass rate of ethanol conversion over various catalysts. (c) Comparison of the catalytic performance with the literature. (d) Kinetic behavior on bm-BEA@oxides. (e) Effect of intimacy on TOF (Turnover Frequency) values. TOFs were calculated at similar controlled conversions (~5%). (f) *In situ* IR spectra for ethanol conversion. (g) Adsorption energies in the DFT study of ethanol or acetaldehyde on active sites (orange, Mg; blue, Si; silver, Al; red, O; brown, C; and white, H). Reprinted with permission from ref. 92, copyright 2023, American Chemical Society.

demonstrating the power of dual-site engineering in single-step alcohol upgrading.

Further advancing zeolite functionality, Liu *et al.*[93] immobilized phosphotungstic acid (HPW) on β-zeolite (Hβ) to catalyze higher alcohol dehydration into jet fuel precursors. The 20% HPW-β composite outperformed pure Hβ, delivering 59.5% selectivity toward C_8–C_{16} hydrocarbons at 240 °C.

This enhancement stemmed from amplified Brønsted acidity, which facilitated oligomerization of a 3 : 2 butanol/hexanol mixture. In parallel work, the same group[95] reengineered ZSM-5 catalysts through hierarchical pore structuring and acidity modulation. Plate-like HZSM-5 with tailored Si/Al ratios and mesoporosity achieved 66.4% C_8–C_{16} selectivity by improving reactant diffusion and active site accessibility. Remarkably, this catalyst maintained its performance in real oil-phase systems, underscoring industrial viability. Innovative hydrophobic engineering of HZSM-5 (Z25) *via* octadecyltrichlorosilane functionalization[96] markedly enhanced C_8–C_{16} selectivity to 80.5%, representing a 29.2% improvement over unmodified counterparts. This performance leap stems from mechanistic contributors. The improved hydrophobicity of the modified catalyst minimizes water poisoning, which is critical for maintaining catalytic activity. The optimized ratio of Brønsted and Lewis acid sites ensures a more balanced catalytic environment. The increased hydrocarbon adsorption capacity allows for better substrate interaction and product formation. Together, these improvements highlight the importance of surface modification in enhancing catalytic performance.

3.2.2 Magnesium-aluminum mixed oxides. The delicate balance between acidic and basic sites in catalysts critically governs the efficiency of ethanol-to-butanol conversion, as mismatched acid-base properties often trigger undesired side reactions.[97] Magnesium–aluminum mixed oxides, derived from calcined layered double hydroxides (LDHs), have emerged as versatile platforms for tuning acid-base characteristics to optimize cascade reactions.[98] The inherent flexibility of LDH precursors allows substitution of Mg^{2+} or Al^{3+} with various metal ions, enabling precise modulation of acidity, basicity, and reducibility to enhance product selectivity.[99] Enhanced basic site density in these systems promotes butanol formation by favoring C–C coupling over acid-driven dehydration pathways.[100] Strategic incorporation of metals such as Ag, Ru, Co, Ni, Cu, or Sn further improves ethanol dehydrogenation efficiency while suppressing competing dehydration reactions under mild conditions.

Pioneering work by Di Cosimo *et al.*[101] pioneered the development of layered double hydroxide(LDH)-derived Mg_yAlO_x catalysts for ethanol coupling, elucidating *n*-butanol formation mechanisms. This methodology is further exemplified by noble metal-doped variants,[107] where Argentum-group elements dominate hydrogenation processes due to their optimal H_2 adsorption-desorption equilibria—a critical feature for hydrogen transfer efficiency. Therefore, noble metals from LDH structures supported on MgAlO catalysts have also been applied to ethanol conversion to butanol to reduce the occur-

rence of competitive side reactions.[74,108] Zhang *et al.*[102] engineered Ag/Mg_4Al-LDO catalysts from MgAl-LDH precursors, achieving 31.7% ethanol conversion with 64.8% butanol selectivity at 350 °C and 0.1 MPa—a 3.4-fold activity increase over unmodified Mg_4Al-LDO. This enhancement stemmed from synergistic interplay between Ag nanoparticles (facilitating ethanol dehydrogenation) and acid-base sites (promoting acetaldehyde condensation). Similarly, Yuan *et al.*[103] demonstrated Ru/MgAl-LDO catalysts achieving 82.6% higher alcohol selectivity at 29.6% conversion, highlighting noble metals' efficacy in directing reaction pathways.

Addressing cost constraints, researchers have pivoted toward transition metal alternatives. Rechi Siqueira *et al.*[104] developed Cu-doped MgAl oxides that achieved 79.6% ethanol conversion with 32.0% butanol selectivity at 350 °C, attributing performance gains to Cu^{2+}-induced redistribution of acid-base sites. Building on this methodology, Lv *et al.*[105] fabricated $Co_nMg_{3-n}AlO_x$ catalysts and investigated the effect of Co doping molar ratio ([Co] = 0.015–0.60) on C_{4-10} alcohols selectivity and ethanol conversion. Increasing the [Co] from 0.015 to 0.15 elevated ethanol conversion from 11.5% to 32.9%, whereas further increasing [Co] to 0.60 markedly suppressed conversion (Fig. 5a). Under milder conditions (250 °C), the optimized $Co_{0.15}Mg_{2.85}AlO_x$ catalyst achieved 95.4% selectivity toward higher alcohols at 32.9% conversion (Fig. 5b). Comparative studies with Mg_3AlO_x revealed that Co^{2+} incorporation significantly accelerates ethanol dehydrogenation and enhances aldol condensation at reduced temperatures (Fig. 5c–f).

Wang *et al.*[106] elucidated synergistic effects in bimetallic systems through the development of Cu-NiMgAlO catalysts. The optimal 2%Cu-NiMgAlO formulation achieved 30.0% ethanol conversion with 62.4% alcohol selectivity, surpassing monometallic analogues *via* dual mechanisms. Enhanced hydrogen transfer capability arose from electronic modulation by Cu^+ species and Cu–Ni alloy formation, while balanced acid-base pair sites facilitated cascade dehydrogenation-condensation (Fig. 6a). When tested on NiMgAlO for 100 h, the catalyst maintained ~20% ethanol conversion and 51–58% *n*-butanol selectivity, beyond which both metrics declined (Fig. 6b). In contrast, the Cu-doped 2%Cu-NiMgAlO exhibited superior activity and stability, sustaining 30% conversion with 62–64% *n*-butanol selectivity for over 200 h without significant deactivation (Fig. 6c), demonstrating exceptional ethanol conversion stability. Comprehensive investigations validate that transition metal-incorporated MgAl oxides serve as economically viable substitutes for noble metal catalysts, where activity-selectivity profiles are governed by synergistic interplay between acid-base bifunctional configurations and redox-active metal centers.

3.2.3 Hydroxyapatite (HAP)-based catalysts. Hydroxyapatite (HAP), with its amphoteric acid-base properties and structural flexibility, has emerged as a versatile catalyst for ethanol upgrading (Table 5). Its unique crystal lattice tolerates cationic substitutions (*e.g.*, Ca^{2+} replaced by Sr^{2+}, Cu^{2+}, or Ni^{2+}), enabling precise tuning of active sites while maintaining

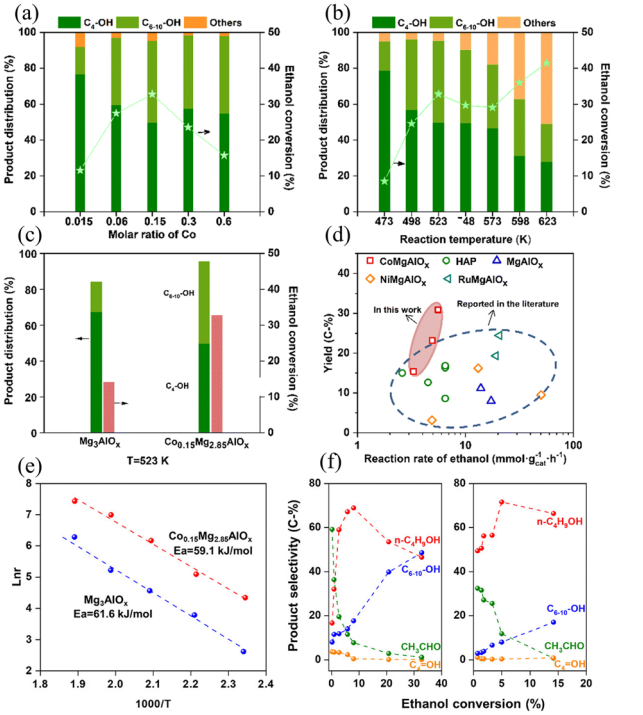

Fig. 5 Catalytic performance. (a) Ethanol conversions over $Co_nMg_{3-n}AlO_x$ catalysts with various Co molar ratios. (b) Ethanol conversions over the $Co_{0.15}Mg_{2.85}AlO_x$ catalyst at various temperatures. (c) Comparison of ethanol conversion and product distribution over $Co_{0.15}Mg_{2.85}AlO_x$ and Mg_3AlO_x catalysts. (d) Yields of C_{4-10} alcohols *versus* the ethanol reaction rate for catalysts described in this work and other catalysts. (e) Arrhenius plots of the reaction rate over the reduced $Co_{0.15}Mg_{2.85}AlO_x$ and Mg_3AlO_x catalysts. (f) Dependence of the product distributions as a function of the ethanol conversion over $Co_{0.15}Mg_{2.85}AlO_x$ and Mg_3AlO_x catalysts. Reprinted with permission from ref. 105 copyright 2023, the Royal Society of Chemistry.

thermal stability and tunable porosity (Fig. 7).[109] The interplay of Lewis acidic Ca^{2+} sites, Brønsted acidic PO-H groups, and basic $(PO_4)^{3-}/OH^-$ moieties create a multifunctional platform for ethanol dehydrogenation and aldol condensation.

Silvester *et al.*[110] demonstrated how Sr^{2+} substitution in HAP enhances higher alcohol selectivity. At 100% Sr substitution (SrAp-100), the catalyst achieved 76.4% total alcohol selectivity at 13.2% ethanol conversion, outperforming Ca-HAP analogs. In a related spectral study by Brasil *et al.*,[111] it was confirmed that the incorporation of Ca^{2+} ions manifested as Lewis acid sites. In addition, the O atoms of the $(PO_4)^{3-}$ and OH-groups are Lewis basic sites, while the oxygen atoms in PO-H are Brønsted acidic sites. Hydroxyapatite (HAP) exhibits acidic characteristics at Ca/P = 1.50 due to phosphate group dominance, whereas increasing the ratio to 1.67 induces alkalinity through hydroxyl enrichment, enabling pH-dependent catalytic behavior modulation. Tsuchida *et al.*[112] systematically correlated HAP's acid-base balance with Ca/P ratios: increasing Ca/P from 1.50 to 1.67 shifted the catalyst from Brønsted-acid-dominant to strongly basic, with butanol selectivity peaking at 62.4% (Ca/P = 1.65). Ogo *et al.*[113] extended this strategy to Sr-

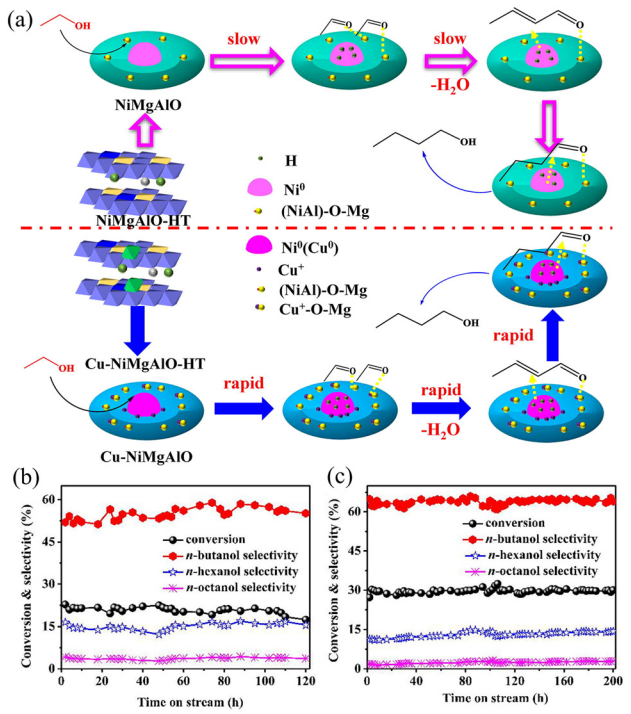

Fig. 6 (a) Conversion of ethanol to *n*-butanol over NiMgAlO and Cu-NiMgAlO catalysts. (b) Stability of NiMgAlO catalyst. (c) Stability of 2% Cu-NiMgAlO catalyst. Reprinted with permission from ref. 106, copyright 2022, Elsevier.

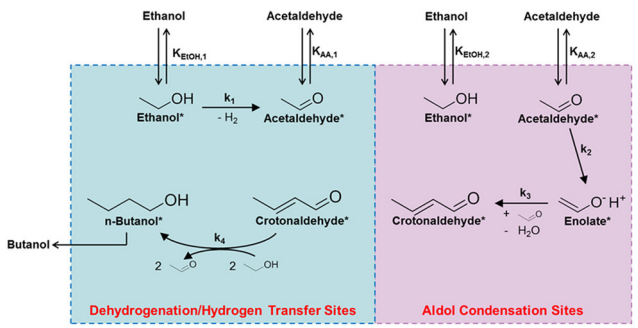

Fig. 7 Proposed Reaction Pathway for the Guerbet Coupling of Ethanol to Butanol over the HAP Catalyst,[109] copyright 2016, American Chemical Society.

HAP systems, where Sr/P = 1.7 yielded 86.4% butanol selectivity by amplifying basic site density—critical for rate-limiting aldol condensation steps.

The initial dehydrogenation and hydrogenation of ethanol under acid-base catalysis affect the conversion of ethanol. To solve the above problems, the catalytic performance of acid-base catalysts can be improved by introducing dehydrogenation-oriented metals such as Ni, Cu, Co, Ag and Ru.[103,105,110] Zhou *et al.*[114] designed Cu-HAP hybrids integrating metallic Cu's hydrogenation activity with HAP's acid-base duality, attaining 86.7% alcohol selectivity at 36.6% ethanol conversion. Selective hydrogenation of crotonaldehyde's unsaturated bonds (C=C/C=O) on Cu sites under H2 atmosphere effectively blocked cyclization byproducts, directing the pathway toward linear Guerbet products. Due to the polar nature of ethanol, it is extremely difficult to separate ethanol from water. Based on the above background, the direct conversion of water–ethanol is of great significance. Addressing water sensitivity in aqueous ethanol systems. Landau *et al.*[115] developed carbonate-incorporated HAP (C-HAP) with reduced hydrophilicity. At 400 °C, C-HAP maintained 74% butanol selectivity despite aqueous feedstocks, outperforming conventional HAP due to weakened water adsorption.

Xue *et al.*[116] addressed a critical challenge in ethanol upgrading—achieving long-chain alcohol synthesis without alkali additives, ligands, or external H_2—by developing a recyclable Ni/biohydroxyapatite (Ni/BioApatite) catalyst. This system defies conventional product distributions, delivering 63.5% selectivity for C_{6+} alcohols at 56.0% ethanol conversion, far exceeding predictions from the Anderson–Schulz–Flory model. The breakthrough stemmed from synergistic interplay between the catalyst's hierarchical porosity and cooperative Niδ$^+$–Ca–[O^{2-}]–Ca active sites, which orchestrated sequential dehydrogenation, condensation, and hydrogenation steps. Building on this foundation, the team[117] engineered Ni/hydroxyapatite (Ni/HAP) catalysts with tunable basicity to overcome the inherent selectivity limitations of stepwise chain growth. By increasing Ni loading on OH$^-$-rich HAP surfaces, they amplified the density of Niδ$^+$ species and Ca–[O^{2-}]–Ca pairs. This optimization yielded the HAP4-0.5Ni catalyst, which achieved 63.6% ethanol conversion with 62.4% C_{6+} alcohol selectivity. Mechanistic studies revealed a linear correlation between ethanol reaction rates and Niδ$^+$ concentration, while C_{6+} alcohol yields scaled with Ca–[O^{2-}]–Ca site density. Synergistic application of operando infrared spectroscopy and density functional theory (DFT) simulations revealed that basic domains preferentially adsorb aldehyde species through charge-transfer interactions, thereby regulating C–C bond formation kinetics and spatial orientation. The proposed reaction pathway demonstrates how spatial organization of redox-active Niδ$^+$ and basic Ca–[O^{2-}]–Ca sites enable cascade reactions in a single catalytic system. The proposed paradigm transcends conventional compromises in catalytic design, demonstrating that multifunctional architectures can concurrently maximize reaction rates and product specificity during alcohol valorization—a previously unattainable feat in heterogeneous catalysis.

3.2.4 Carbon materials as advanced catalyst supports. Lignin, the second most abundant biopolymer on Earth, has emerged as a sustainable precursor for synthesizing functional carbon materials due to its high carbon content (~60%), three-dimensional aromatic network, and tunable functional groups (methoxy, hydroxyl, carboxyl, *etc.*).[118–122] These inherent properties enable the fabrication of lignin-derived carbons with tailored porosity, high surface areas (>1000 m^2 g^{-1}), and rich defect structures—critical features for catalytic applications.[123–128] Strategic nitrogen doping further enhances these materials by introducing pyridinic and graphitic N sites,

which improve metal dispersion and strengthen metal-support interactions.[129–132]

In addition, nickel-based catalysts with nanostructures can achieve excellent ethanol conversion and butanol selectivity under mild reaction conditions, and exhibit outstanding dehydrogenation performance.[133,134] Fei *et al.*[135] pioneered NiSn bimetallic nanoparticles encapsulated in N-doped lignin carbon (NiSn@NC), achieving 68.5% ethanol conversion with 46.4% C_{4+} alcohol yield. The Sn/N co-doping strategy optimized Ni electronic structure and dispersion, while even after running for four cycles, it still demonstrates stable and outstanding performance. Therefore, NiSn@NC the bimetallic catalyst is able to react stably in aqueous phase the carbon matrix stabilized the catalyst through four operational cycles in aqueous phase. Lin's team[136] advanced this approach using Zn/N co-doped Ni catalysts (NiZn@NC) derived from paper mill lignin (Fig. 8). The optimized $Ni_{20}Zn_1$@NC exhibited 75.2% conversion and 55.4% C_{4+} selectivity, where Zn doping suppressed methane formation and carbon deposition by creating electron-rich Ni sites.

Xu *et al.*[137] systematically investigated nitrogen source effects on catalyst performance. Diethylenetriamine (DETA)-modified Ni@NC demonstrated superior activity (81.1% conversion, 43.5% selectivity), outperforming counterparts using polyethyleneimine (PEI) or L-histidine (Fig. 9b and c). DETA's branched structure facilitated optimal charge redistribution, forming Ni–N–C configurations that minimized over-adsorption of intermediates while enhancing metal-support synergy (Fig. 9a and d).

These lignin-derived catalytic systems transcend conventional limitations through a trifecta of atomic-level synergies: spatial confinement in carbon matrices suppresses metal sintering, heteroatom doping dynamically modulates electronic states to create adaptive active sites, and engineered defects at grain boundaries selectively stabilize reaction intermediates through tailored adsorption geometries. The work establishes lignin carbons as next-generation catalyst supports, merging sustainability with performance rivaling conventional activated carbons. The demonstrated strategies—from precursor functionalization to multimetallic design—provide a blueprint for developing biomass-derived catalysts for circular biorefineries.

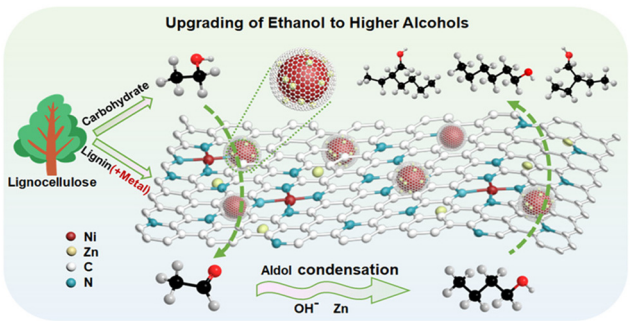

Fig. 8 Reaction pathway for ethanol upgrading to higher alcohols over lignin-derived carbon-encapsulated NiZn@NC catalysts,[136] copyright 2022, American Chemical Society.

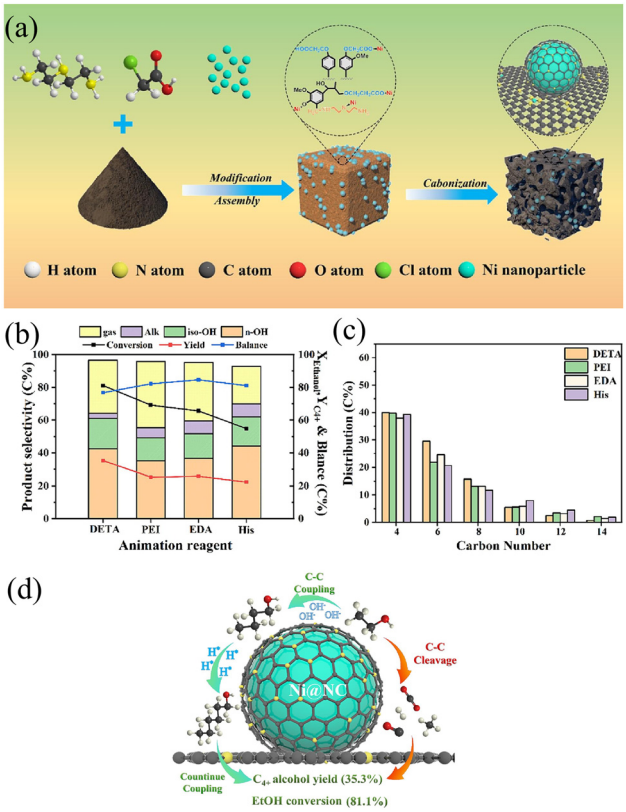

Fig. 9 (a) Synthesis of lignin-derived carbon-encapsulated Ni catalysts with nitrogen coordination (Ni@NC). (b) Effect of 1/2-Ni_{20}@NC catalysts modified with different aminating reagents on the conversion of ethanol to higher alcohols: ethanol conversion, higher alcohols yield, product selectivity, and (c) carbon balance. (d) Reaction pathway of ethanol to higher alcohols. Reprinted with permission from ref. 137 copyright 2024, American Chemical Society.

The versatility of biomass-derived carbon materials extends beyond lignin, with diverse precursors enabling tailored catalyst designs for ethanol upgrading. Chen *et al.*[138] demonstrated this potential using chitosan—a biopolymer rich in amino and hydroxyl groups—as a support for Sn–Ni bimetallic catalysts. The Sn–Ni/CS-500-1/1 system achieved 60% ethanol conversion and >85% selectivity toward higher alcohols at 230 °C, where Sn doping induced electron-rich Ni sites that weakened aldehyde intermediate adsorption, effectively suppressing gaseous byproducts. Zhong's team[139] further advanced aqueous-phase catalysis through sodium glutamate-derived Ni@C composites, which exhibited 85.7% C_{4+} alcohol selectivity at 40.8% conversion. The catalyst's unique phase-transfer capability, coupled with alkali sites in the carbon matrix, facilitated secondary carbon coupling to yield C_8–C_{16} alcohols with an iso/*n*-OH ratio of 1.86, directly compatible with hydrodeoxygenation into jet fuels.

Small-molecule carbon precursors like citric acid have also proven effective. The NiMo@C catalyst prepared by Liao *et al.*[140] has pushed boundaries further, achieving 89.4%

ethanol conversion and 84.6% higher alcohol selectivity. Introducing molybdenum into Ni-based systems generated hydroxyl-rich NiMo-O interfaces with amphiphilic properties, which selectively adsorbed lipid-soluble aldehyde intermediates to facilitate chain elongation toward C_8–C_{16} alcohols. To study the interaction between material carbon and inorganic metals, Wu *et al.*[141] engineered Ni–Sn catalysts supported on hybrid carbon-TiO_2 matrices, where the amphoteric surface chemistry of the support optimized metal nanoparticle electronic states, resulting in enhanced ethanol conversion (70.6%) and C_{6+} alcohol selectivity (57.5%). Further research indicates that the improvement in catalytic performance is mainly due to the promoting effect of the amphiphilic NiSn@C-TiO_2 catalyst on emulsion catalysis, through which the process from the self-coupling reaction of water-based ethanol to the intermolecular cross-coupling reaction at the oil/water interface is greatly accelerated. Cai *et al.*[142] engineered amphiphilic NiSn@C-MgO catalysts that stabilized emulsions for cross-coupling reactions between ethanol and C_{4+} intermediates. At 73.3% conversion, the system delivered 60.9% selectivity for C_{6+} alcohols, with structural analysis revealing temperature-dependent carbon shell evolution as a critical performance factor (Fig. 10).

Innovative surface engineering strategies have unlocked unprecedented performance. Gu *et al.*[65] revolutionized long-chain alcohol synthesis through sulfur-modified Ni@C–$S_{1/30}$ catalysts. Screening of Ni@C–S_x catalysts with varying S/Ni molar ratios at 180 °C (Fig. 11a and b) identified Ni@C–$S_{1/30}$ as optimal. Subsequent two-stage intensification—initial reaction at 180 °C followed by temperature-ramped maintenance (6 h)—drove near-complete ethanol conversion (99.1%) with 74.2% C_{6+} alcohol selectivity, defying conventional Anderson-Schulz-Flory distributions (Fig. 11c). This breakthrough originates from selective sulfur masking of Ni sites, which simultaneously suppresses C–C cleavage and stabilizes aldehydes to redirect pathways toward chain growth. The chain propagation profile with α = 0.58 confirms preferential formation of long-chain products (Fig. 11e and g). Ternary analysis correlating conversion, LAS yield, and selectivity positions Ni@C-$S_{1/30}$ beyond reported catalysts in ethanol upgrading efficiency and product control (Fig. 11d). Stability testing demonstrated retained high activity/selectivity over 5 cycles (Fig. 11f), confirming structural robustness for continuous-flow applications.

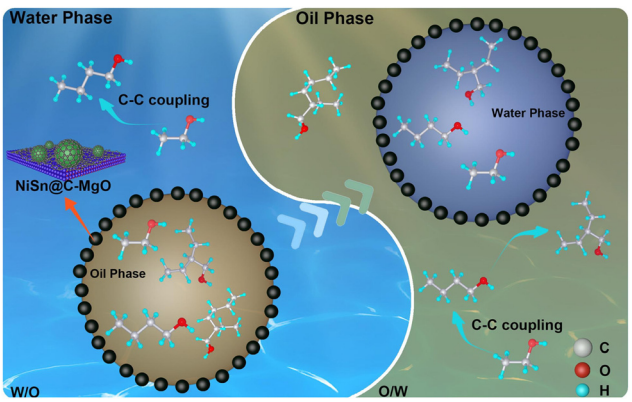

Fig. 10 Schematic illustration of the ethanol upgrading reaction pathway over NiSn@C-MgO catalysts. NiSn@C-MgO catalysts can stabilize oil–water emulsions and catalyze the reactions at the oil–water interface; the product migrates in both the oil and water phases as the reaction proceeds,[142] copyright 2023, Elsevier.

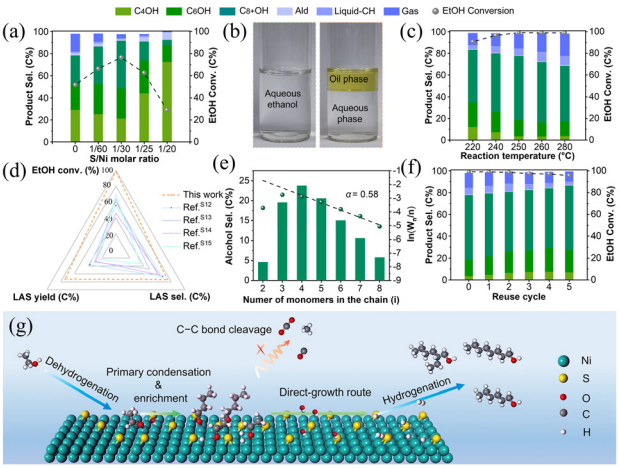

Fig. 11 (a) EtOH conversion and product selectivity over Ni@C–S_x catalysts with different S/Ni molar ratios at 180 °C. (b) Photographs of aqueous EtOH feedstock (left) and obtained liquid products (right). (c) Catalytic performance of the Ni@C–$S_{1/30}$ catalyst in the two-stage intensification process. (d) Catalytic performance comparison among Ni@C–$S_{1/30}$ catalyst and other previously reported catalysts. (e) Detailed alcohol distribution, step-growth plot and α value over Ni@C–$S_{1/30}$ catalyst under optimized reaction conditions. (f) Stability test for Ni@C–$S_{1/30}$ catalyst. (g) Schematic illustration for the role of sulfur in promoting upgrading of EtOH to LAS. Reprinted with permission from ref. 65, copyright 2023, Springer Nature.

The adaptability of carbon supports is further exemplified by polyacrylamide-derived catalysts. Zheng *et al.*[143] developed hcp-Ni@C catalysts active at <100 °C, where surfactant-induced hexagonal close-packed Ni structures lowered the energy barrier for ethanol dehydrogenation—a rate-determining step in aqueous environments.

Gu's nitrogen-doped Ni@NC catalysts[144] suppressed methane formation (1.6% selectivity) while achieving 74.8% ethanol conversion, demonstrating scalability through 100-fold reactor expansions. Nitrogen's electronic modulation strengthened Ni-intermediate interactions, favoring alcohol chain growth over decomposition. Pang *et al.*[146] prepared a catalyst of 4%Ir and 4%Ni/MC from a precursor with sodium bicarbonate as the carbon carrier. Initial catalytic testing revealed limited efficacy, with ethanol conversion reaching merely 3.0% during valorization into long-chain alcohols—a performance deficit attributed to suboptimal active site configuration. In order to improve the catalytic performance of this type of catalyst, Yuan *et al.*[145] developed a nitrogen-doped carbon-modified copper-based catalyst using sodium carbonate salt solution as the carbon carrier precursor and melamine/copper–magnesium–aluminum layered dihydroxide

complex as the precursor, and conducted an in-depth study on its catalytic performance in ethanol conversion. Under the reaction conditions of 250 °C and 2 MPa, this catalyst achieved an ethanol conversion rate of 63% and a high carbon alcohol selectivity of 82%. N-doping of carbon matrices induce dual functionalities, which enhanced spatial distribution of Cu nanoparticles through defect anchoring, and electronic modulation generating Cu^{+}–Ov (oxygen vacancy) pairs at metal-support junctions. This interfacial synergy elevates catalytic turnover frequency while enabling cascade dehydrogenation-condensation steps in ethanol upgrading.

Petrochemical residues, including petroleum asphalt and heavy oils, serve as critical precursors for synthesizing porous carbon materials through high-temperature pyrolysis and activation. Pyrolysis of petroleum residues generates hierarchical carbon morphologies—including microporous activated carbons, aligned nanotubes, and ultralight aerogels[150–160]—featuring three-dimensional porous frameworks that optimize metal nanoparticle immobilization. Such structural advantages improve metal-support electronic communication,[161] allowing these carbons to outperform conventional materials in oxygen evolution and Fischer–Tropsch synthesis.[162–172]

Jiang *et al.*[147] exemplified this potential with a Cu-CeO_2/activated carbon (AC) catalyst prepared *via* impregnation. The CeO_2/Cu system exhibited exceptional activity through cooperative interactions: ceria suppressed Cu sintering *via* strong metal-support bonding, while its surface basicity facilitated aldol coupling of acetaldehyde intermediates. Building on this, Wang *et al.*[148] systematically compared Ni-CeO_2 catalysts on varied carbon supports (AC, carbon black, CNTs, CMK-3). Activated carbon emerged as the optimal carrier, delivering 27.2% ethanol conversion with 85.6% C_4–C_8 alcohol selectivity. AC's high surface area and functional groups stabilized balanced Ni^0/Ni^{2+} sites and acid-base pairs, while strong Ni-CeO_2 interactions inhibited carbonate formation, ensuring long-term stability. Further refining this approach, the same team[149] engineered Ni-CeO_2 within microporous carbon nanotubes (CNTs). Confinement effects in narrowed CNT channels concentrated acetaldehyde intermediates near CeO_2-generated acid-base pairs, synergistically enhancing both ethanol conversion and 1-butanol selectivity. The microporous architecture not only enriched reactants but also modulated electronic interactions between Ni and CeO_2, demonstrating how nanoscale confinement can reprogram catalytic behavior. These studies collectively underscore petrochemical carbons' dual role as structural scaffolds and electronic modulators. By marrying tunable porosity with metal-support interactions, they bridge the gap between industrial feedstock utilization and precision catalysis—a paradigm increasingly relevant in sustainable fuel synthesis.

Noble metal catalysts drive molecular-level precise catalysis with single-atom active centers, while non-noble metal catalysts rely on multimetallic synergistic effects.[173,174] This difference in active sites extends to the support layer. Homogeneous catalytic systems follow a continuous pathway of "dehydrogenation–condensation–hydrogenation",[175] whereas heterogeneous catalysts generate parallel reactions due to interfacial complexity.[145] For example, Mg–Al oxide and Hydroxyapatite catalysts can suppress by-products by optimizing the density of basic sites,[176–178] and carbon-based catalysts can promote the diffusion of long-chain intermediates through mesoporous structures, inhibit C–C bond cleavage, and enhance the selectivity of long-chain alcohols.[179] The difference in these pathways is essentially determined by the uniformity of active site distribution—the molecular-level regulation capability of homogeneous systems gives them an advantage in the selectivity of short-chain products, while the interfacial diversity of heterogeneous catalysis is more conducive to long-chain growth.[180]

3.3 Comparative analysis of atom economy and environmental factor (*E*-factor) across catalytic routes

The comparison of atom economy and environmental factor (*E*-factor) is critical for evaluating the sustainability of catalytic technologies in converting ethanol to higher alcohols.[181] Atom economy reflects the efficiency of converting reactant atoms into target products, while the *E*-factor defines the mass (kg) of waste generated per kg of product, collectively reflecting the green chemistry characteristics of catalytic systems.[182,183]

3.3.1 Waste generation differences between homogeneous and heterogeneous catalysis. Homogeneous catalytic systems (*e.g.*, iridium/ruthenium-based catalysts) generally exhibit higher *E*-factors, primarily due to the use of organic ligands and solvents.[184] For instance, the $[Ir(OAc)_3]$-L10 system (Table 2, entry 2), requires phenanthroline disulfonate ligands, generating a considerable amount of waste per kg of product. Additionally, homogeneous catalysts are difficult to recycle, with unrecovered noble metal residues further increasing environmental burdens. In contrast, heterogeneous catalytic systems (*e.g.*, Mg–Al mixed oxides) demonstrate significant advantages: the Cu-NiMgAlO (Table 4, entry 7) catalyst in a fixed-bed reactor can remain active for 200 hours at 250 °C, recyclable *via* simple filtration, drastically reducing waste generation.

3.3.2 Environmental performance comparison between noble and non-precious metal catalysts. Noble metal catalysts (*e.g.*, Rh, Ir) exhibit higher *E*-factors due to the high cost of ligand synthesis and complex recovery processes. For example, while the Ir-$[Tp'Ni(\mu\text{-}OH)]_2$ (Table 2, entry 3) system achieves 99% selectivity for 1-butanol with high atom economy; however, decomposition products from its ruthenium ligand complicate waste management. Non-precious metal systems (*e.g.*, Co-doped Mg–Al oxides) align better with sustainability goals: $Co_{0.15}Mg_{2.85}AlO_x$ (Table 4, entry 6), achieve 95.4% higher alcohol selectivity with a lower *E*-factor, eliminating the need for additional ligands and significantly reducing waste.

From a life cycle perspective, non-precious metal catalysts (*e.g.*, Ni/CeO_2@CNTs) (Table 6, entry 15) show lower toxicity and eliminate complex noble metal recovery processes, further reducing environmental loads. These findings provide a theoretical basis for designing catalytic systems with high atom economy and low *E*-factors—e.g., optimizing reaction pathways *via* acid-base site synergy (*e.g.*, hydroxyapatite cata-

Table 2 Homogeneous catalysts catalyze the upgrading of ethanol to high-carbon alcohols

Entry	Catalyst	Temperature	Reaction time	Reactor	Conv./%	Sel./%	Ref.
1	[Ir(acac)(cod)]	120 °C	15 h	Reaction still	41.0	51.0	67
2	[Ir(OAc)$_3$]-L10 (1 : 8)	150 °C	12 h	Reaction still	54.0	91.0	68
3	Ir-[Tp′Ni(μ-OH)]$_2$(1 : 25)	150 °C	24 h	Reaction still	37.0	>99.0	69
4	[RuCl(η^6-*p*-cymene)]Cl	150 °C	4 h	Reaction still	22.1	93.6	70
5	[RuCl$_2$(η^6-*p*-cymene)]$_2$	150 °C	4 h	Reaction still	31.4	92.7	71
6	[Ru(bipy^{OH})]	80 °C	18 h	Reaction still	49.1	57.0	72
7	N,N,N-Ru(II)	150 °C	2 h	Reaction still	53.0	80.0	73
8	[Ru]-6	150 °C	40 h	Reaction still	73.4	>99.0	74
9	Ru(5-CH$_3$-bpi)(PPh$_3$)$_2$Cl	150 °C	2 h	Reaction still	—	65.0	75
10	[HN(CH$_2$CH$_2$P^{i}Pr$_2$)$_2$]Mn(CO)$_2$Br	160 °C	168 h	Reaction still	11.2	92.0	76
11	[HN(CH$_2$CH$_2$PPh$_2$)$_2$]Mn(CO)$_2$Br	150 °C	24 h	Reaction still	72.0	69.5	77
12	[Ru]–[Mn]	180 °C	24 h	Reaction still	—	70.0	78

Conv.: conversion of ethanol; Sel.: selectivity of higher alcohol; Ref.: references.

lysts) or carbon-based support confinement effects (*e.g.*, sulfur-modified Ni@C-S$_{1/30}$) (Table 6, entry 10)—to simultaneously enhance selectivity and environmental benefits.

4 Applications and functional properties of higher alcohols

Higher alcohols exhibit unique value across diverse fields due to their tunable carbon chain lengths and functional groups. As the carbon chain extends from short to long, gradients in physicochemical properties—such as hydrophobicity, boiling point, and viscosity—drive applications ranging from energy fuels to fine chemicals.

4.1 Liquid fuel applications

The environmental hazards and unsustainability of fossil fuels have spurred global exploration of renewable alternatives. While hybrid systems, electric drives, fuel cell, and solar technologies[185–188] face commercialization challenges due to energy density and infrastructure limitations,[189,190] internal combustion engines remain central to land transport, necessitating cleaner fuel solutions.[191] Oxygenated alcohols, particularly ethanol and C_{4+} higher alcohols, emerge as critical candidates. Their molecular oxygen content optimizes combustion, reducing particulate matter and unburned hydrocarbon emissions.[192,193] Bio-derived from sugarcane, oil crops, or waste biomass, these alcohols offer carbon cycle advantages.[194–197] Ethanol and C_{4+} alcohols dominate automotive fuels due to mature biosynthesis pathways, high octane ratings, and flame propagation rates.[198,199] However, their lower energy density and challenges in cold-start performance demand synergistic optimization of fuel properties and engine parameters for scalable adoption.[200–202]

4.2 Aviation fuel precursors

Higher alcohols are gaining traction as sustainable aviation fuel (SAF) precursors.[203] Through deoxygenation and isomerization, C_8–C_{16} alcohols convert to branched alkanes with energy densities matching conventional jet fuels.[21,204] For instance, a 20% phosphotungstic acid-loaded β-zeolite (20% HPW-β) (Table 3, entry 4) achieved 59.5% selectivity toward C_8–C_{16} hydrocarbons, owing to enhanced Brønsted acidity and synergistic acid-base sites.[93] Further optimization of zeolite structure *via* hierarchical porous engineering in plate-like HZSM-5 (Table 4, entry 6) boosted selectivity to 66.4%, demonstrating that shortened diffusion paths and tailored acidity synergistically promote oligomerization.[95] Notably, hydrophobic modification of HZSM-5 with octadecyltrichlorosilane (Z25-OTS) (Table 3, entry 7) increased C_8–C_{16} selectivity to 80.5%, attributed to reduced water adsorption and enhanced olefin accumulation on the catalyst surface.[96] Mechanistic insights were deepened by integrating kinetic modeling of alcohol-to-jet (ATJ) fuels. Experimental ignition delay measurements revealed that highly branched isoparaffins in ATJ fuels exhibit low oxidation reactivity at low temperatures, necessitat-

Table 3 Zeolites catalysts catalyze the upgrading of ethanol to higher alcohols

Entry	Catalyst	Temperature	Reaction time	Reactor	Conv./%	Sel./%	Ref.
1	Rb-LiX	420 °C	$W/F_{ethanol}$ = 5.6(h g) mol^{-1}	Fixed-bed	20.8	40.9	64
2	Pd/Zr-Beta	235 °C	WHSV = 0.4–0.8 h^{-1}	Fixed-bed	12.5	8.6	91
3	bm-BEA@oxides	310 °C	WHSV = 2.3 h^{-1}	Fixed-bed	24.0	81.0	92
4	20%HPW-β	240 °C	12 h	Reaction still	—	59.5(C_8–C_{16})	93
5	Pt-Y/Beta	200 °C	WHSV = 2 h^{-1}	Fixed-bed	34.0	68.0	94
6	HZSM-5	260 °C	12 h	Reaction still	—	66.4(C_8–C_{16})	95
7	HZSM-5(Z25-OTS)	260 °C	12 h	Reaction still	—	80.5(C_8–C_{16})	96

Conv.: conversion of ethanol; WHSV: weight hour space velocity; Sel.: selectivity of higher alcohol; Ref.: references.

Table 4 Magnesium–aluminum mixed oxides catalyst catalyzes the upgrading of ethanol to high-carbon alcohol

Entry	Catalyst	Temperature	Reaction time	Reactor	Conv./%	Sel./%	Ref.
1	Mg_4Al-LDO	350 °C	LHSV = 6 mL (h g)$^{-1}$	Fixed-bed	9.3	47.8	102
2	Ag/Mg_4Al-LDO	350 °C	LHSV = 6 mL (h g)$^{-1}$	Fixed-bed	31.7	64.8	102
3	Ru/Mg_3Al-LDO	350 °C	WHSV = 3.2 h^{-1}	Fixed-bed	29.6	82.6	103
4	Cu-MgAlO	350 °C	5 h	Reaction still	79.6	32.0	104
5	Mg_3AlO_x	250 °C	WHSV = 0.96 h^{-1}	Fixed-bed	14.2	83.3	105
6	$Co_{0.15}Mg_{2.85}AlO_x$	250 °C	WHSV = 0.96 h^{-1}	Fixed-bed	32.9	95.4	105
7	2%Cu-NiMgAlO	250 °C	200 h	Fixed-bed	30.0	64.2	106

Conv.: conversion of ethanol; LHSV/WHSV: liquid/weight hour space velocity; Sel.: selectivity of higher alcohol; Ref.: references.

Table 5 Hydroxyapatite catalyst catalyzes the upgrading of ethanol to high-carbon alcohol

Entey	Catalyst	Temperature	Reaction time	Reactor	Conv./%	Sel./%	Ref.
1	SrAp-100	400 °C	4 h	Fixed-bed	13.2	76.4	110
2	Ca-HAP-3(1.65)	400 °C	GHSV = 10 000 h^{-1}	Fixed-bed	21.2	62.4	112
3	Sr-HAP-4(1.70)	300 °C,	$W/F_{ethanol}$ = 130(h g) mol^{-1}	Fixed-bed	11.3	86.4	113
4	Cu-HAP	250 °C	0.5 h	Fixed-bed	36.6	86.7	114
5	C-HAP	400 °C	WHSV = 0.5 h^{-1}	Fixed-bed	31.0	74.0	115
6	Ni/HAP	200 °C	24 h	Reaction still	56.0	63.5(C_{6+})	116
7	HAP4-0.5Ni	220 °C	WHSV = 0.7 h^{-1}	Fixed-bed	63.6	62.4	117

Conv.: conversion of ethanol; GHSV/WHSV: gas/weight hour space velocity; Sel.: selectivity of higher alcohol; Ref.: references.

Table 6 Carbon materials catalyst supports catalysts catalyze the upgrading of ethanol to high-carbon alcohols

Entry	Catalyst	Temperature	Reaction time	Reactor	Conv./%	Sel./%	Ref.
1	$Ni_{20}Sn_1$@NC	250 °C	24 h	Reaction still	68.5	46.4	135
2	$Ni_{20}Zn$@NC	250 °C	24 h	Reaction still	72.5	55.4	136
3	1/2Ni_{20}@NC-DETA	250 °C	24 h	Reaction still	81.1	43.5	137
4	Sn-Ni/CS	230 °C	12 h	Reaction still	60	>85	138
5	Ni@C-NaGlu	250 °C	24 h	Reaction still	40.8	85.7	139
6	NiMo@C	240 °C	12 h	Reaction still	89.7	84.6	140
7	NiSn@C-TiO_2	250 °C	18 h	Reaction still	70.6	57.5(C_{6+})	141
8	Ni-Sn@C-MgO	250 °C	12 h	Reaction still	73.3	60.9(C_{6+})	142
9	hcp/fcc-Ni@C	<100 °C	12 h	Reaction still	17.6	>99	143
10	Ni@C-$S_{1/30}$	180 °C–250 °C	12 h	Reaction still	99.1	74.2(C_{6+})	65
11	Ni@NC-2-500	230 °C	12 h	Reaction still	74.8	65.9	144
12	Cu-NC-2-550	250 °C	LHSV = 3.6 mL (h g_{cat})$^{-1}$	Fixed-bed	63.0	82.0	145
13	4%Ir4%Ni/MC	200 °C	24 h	Reaction still	3.0	64.7	146
14	Cu-CeO_2/AC	250 °C	48 h	Fixed-bed	46.2	41.3	147
15	NiCeO_2/AC	230 °C	24 h	Reaction still	27.2	85.6	148
16	Ni/CeO_2@CNTs	230 °C	24 h	Reaction still	27.0	91.1	149

Conv.: conversion of ethanol; LHSV: liquid hour space velocity; Sel.: selectivity of higher alcohol; Ref.: references.

ing catalyst designs that promote hydrodeoxygenation and isomerization. A data-driven kinetic mechanism (ARLMech-HC-ATJ)[205] showed that tuning Brønsted/Lewis acid ratios in hydrophobic zeolites accelerates the rate-determining C–C coupling step, aligning with the observed selectivity improvements.

Gevo Inc. has established significant expertise in renewable fuel technologies, particularly through developing proprietary systems that upgrade biomass-derived feedstocks into sustainable alternatives to fossil-based products. The company's intellectual property portfolio includes innovations spanning microbial strain engineering for enhanced bioconversion efficiency, as well as separation methodologies critical for recovering target compounds like isobutanol. A strategic focus involves advancing Sustainable Aviation Fuel (SAF) production platforms, where patented processes categorized under C10L5/44 (oxygenated fuel compositions) and C12P7/08 (microbial hydrocarbon synthesis) enable the transformation of fusel oil streams into viable jet fuel components.[206] Gevo's ETJ process employs Alcohol-to-Jet (ATJ) pathways, which directly correlate with our discussion on ethanol upgrading *via* Guerbet coupling and aldol condensation (section 2.2). Their partnership with Axens utilizes proprietary catalysts for C–C chain extension, echoing our emphasis on acid-base synergy and metal-

Table 7 Comparative analysis of carbon chain elongation characteristics and applications of higher alcohols

Carbon range	Representative alcohols	Core characteristics	Main application areas	Ref.
C_4	*n*-Butanol, isobutanol	High volatility, limited water solubility	Plasticizers, coatings, fuel additives	217–219
C_5–C_8	Hexanol, octanol	Mild odor, strong lipophilicity	Extractants, solvents, stabilizers	220–222
C_9–C_{10}	Nonanol, decanol	Low water solubility, high stability	Surfactants, lubricants	223 and 224
C_{11}–C_{14}	Lauryl alcohol, myristyl alcohol	High phase change latent heat	Phase change materials	225 and 226
C_{15}–C_{18}	Cetyl alcohol, stearyl alcohol	Superior emulsifying/lubricating capacity	Emulsifiers, lubricants	215 and 227

support interactions in catalyst design.[207] Gevo's Net-Zero 1 (NZ1) facility (65 million gallons/year SAF capacity) demonstrates large-scale viability of ethanol-derived SAF.[208–210] Key to their success is the integration of *in situ* product separation and renewable energy-powered decarbonization.

These SAFs exhibit high cetane numbers, shortening ignition delays and reducing in-flight combustion risks. Residual oxygen groups in their structure enhance soot precursor oxidation, cutting particulate emissions compared to traditional fuels.[211] Crucially, their production aligns with carbon-negative pathways: syngas-derived Fischer–Tropsch synthesis,[212] ethanol coupling,[213] Cross-coupling of ethylene glycol and primary alcohols,[214] and CO_2 hydrogenation achieving CO_2-to-alcohol[35] conversion offer scalable routes to "net-zero aviation fuels".

4.3 High-value chemical applications

Higher alcohols exhibit properties directly governed by carbon chain length, determining their industrial utility (Table 7). Shorter-chain variants (C_4–C_8, *e.g.*, *n*-butanol, hexanol) show high volatility and lipophilicity, making them ideal for fuel additives, extractants, and solvents. Mid-chain alcohols (C_9–C_{14}, *e.g.*, decanol, myristyl alcohol) display low water solubility and thermal stability, suitable for surfactants and lubricants. The C_{11}–C_{14} homologs like lauryl alcohol utilize significant phase-change latent heat for thermal energy storage, with phase transition temperatures optimal for building climate control. Long-chain alcohols (C_{15}–C_{18}, *e.g.*, cetyl alcohol) provide superior emulsification and lubrication. Cetyl-stearyl alcohol mixtures form stable lamellar liquid crystals in emulsions, enhancing stability and texture. Mechanistically, stearyl alcohol reduces skin water loss in cosmetics, while cetyl alcohol improves hair smoothness in conditioners.[215,216] These applications hinge on higher alcohols' dual characteristics: hydrophobic chains for physical functionality and hydroxyl groups for reactivity. By engineering chain length, branching, and derivatization, higher alcohols bridge energy, materials science, and biotechnology, offering versatile solutions for sustainable innovation.

5 Summary and perspectives

The pressing challenge of reducing China's reliance on fossil fuels demands innovative solutions for biofuel development, particularly in upgrading bioethanol—a renewable yet suboptimal fuel due to its corrosiveness and low energy density—into value-added higher alcohols. This review analysis focuses on C–C bond formation paradigms, particularly the concerted dehydrogenation–hydrogenation cycles and aldol-based chain growth mechanisms that underpin modern ethanol upgrading technologies. Homogeneous catalysts while achieving molecular precision under mild conditions, face scalability hurdles due to noble metal dependency and solvent limitations. Heterogeneous systems, leveraging support engineering and metal-carrier synergies, offer improved stability and cost-effectiveness but contend with mass transfer inefficiencies and selectivity challenges. Despite their adjustable pore geometries and hydrothermal stability, carbon-supported catalysts face commercialization challenges including nanoparticle coalescence and energy-intensive synthesis.

Emerging catalysts such as single-atom catalysts (SACs) and metal-organic framework (MOF)-based catalytic systems have garnered significant attention in the field of catalysis.[228] However, their direct application in the Guerbet coupling of ethanol remains underexplored, despite their inherent properties holding great promise for promoting this reaction. Atomically dispersed metal sites, as reported in the literature,[229] feature unique "isolated active centers" that may enable synergistic regulation of dehydrogenation and C–C coupling,[230–232] alongside hydrogenation of aldehyde intermediates to facilitate the transformation of lower alcohols into higher alcohols. Meanwhile, the porous confinement characteristics of MOF materials are anticipated to precisely stabilize acetaldehyde intermediates within the catalytic system under mild conditions,[233] predicting their exceptional potential in selectivity control for long-chain alcohol synthesis.

A critical frontier lies in designing catalysts that harmonize dehydrogenation activity with selective C–C coupling. Non-precious metals (*e.g.*, Ni, Cu) on tailored supports now rival noble metals by optimizing metal-support charge transfer, while balanced Lewis acid-base pairs—acid sites for ethanol activation and base sites to suppress C–C cleavage—enable efficient chain growth. Notably, C_8–C_{16} alcohols produced *via* these systems exhibit ideal iso/*n*-OH ratios, positioning them as direct precursors for hydrodeoxygenation into sustainable aviation fuels (SAFs). This dual-output strategy—simultaneously addressing transportation and aviation needs—could revolutionize biomass utilization. The convergence of confinement effects in hierarchical carbons, electronic modulation *via* doping, and biomass-derived support systems presents a transformative opportunity. By resolving the tension between catalytic accuracy and industrial practicality, the next-generation system can position bioethanol as an alternative to

gasoline and even serve as the cornerstone of a renewable aviation economy. Realizing this vision requires joint efforts in clarifying the basic mechanisms, pilot-scale verification, and a policy framework that encourages the use of sustainable aviation fuel (SAF)—all three of which are crucial for the decarbonization of land and air transportation.

Author contributions

Rongqi Lei, Zetong Chen, Quanzhou Xu, Nan Wang: conceptualization, original draft writing, and investigation. Yanlin Qin, Tiejun Wang: reviewing and editing writing. Xuliang Lin, Xueqing Qiu: funding acquisition, supervision, correspondence, and resources.

Conflicts of interest

The authors declare no competing interests.

Data availability

No primary research results, software or code have been included and no new data were generated or analysed as part of this review.

Acknowledgements

We thank all publishers, journals, and authors who have allowed us to reprint figures and data for our critical review. This work was sponsored by the National Natural Science Foundation of China (U23A6005, 22038004 and 22178069).

References

1 Y. Chen, X. Wang, X.-Y. Li, R. K. Miao, J. Dong, Z. Zhao, C. Liu, J. E. Huang, J. Wu, S. Chu, W. Ni, Z. Guo, Y. Xu, P. Ou, B. Xu, Y. Hou, D. Sinton and E. H. Sargent, *Nat. Catal.*, 2025, **8**, 239–247.
2 C. Samaras, *Nat. Clim. Change*, 2025, **15**, 467–468.
3 C. D. Díaz-Marín and E. N. Wang, *Joule*, 2025, **9**, 101849.
4 M. Filonchyk, M. P. Peterson, L. Zhang, V. Hurynovich and Y. He, *Sci. Total Environ.*, 2024, **935**, 173359.
5 R. Murphy, *Energy Res. Soc. Sci.*, 2024, **108**, 103390.
6 R. Nagaj, B. Gajdzik, R. Wolniak and W. W. Grebski, *Energies*, 2024, **17**, 1245.
7 D. Navia Simon and L. Diaz Anadon, *Nat. Energy*, 2025, **10**, 291–292.
8 Y. Yuan, X. Li, X. Sun, Y. Sun, M. Yang, B. Liu, D. Yang, H. Li and Y. Liu, *Nano Energy*, 2025, **136**, 110727.
9 F. Zhou, J. Yu, C. Wu, J. Fu, J. Liu and X. Duan, *Sci. Total Environ.*, 2024, **913**, 169708.
10 G. Konwar, R. Banik and S. R. Geed, *Chem. Eng. J.*, 2025, **515**, 163456.
11 A. K. Agarwal, C. Mounaïm-Rousselle, P. Brequigny, A. Dhar, C. Hespel, C. Patel, D. K. Srivastava, G. Duraisamy, L. Le Moyne, N. Sharma, N. Labhasetwar, P. Singh, P. Das, P. K. Panigrahi, P. C. Shukla, P. Sakthivel, S. V. Mohan, S. Panigrahy, S. Sen and H. Valera, *Prog. Energy Combust. Sci.*, 2025, **110**, 101236.
12 M. Nour, W. Zhang, M. Cui, J. Fu, X. Luo, S. Qiu, X. Li and M. Xu, *Energy Convers. Manage.*, 2025, **339**, 119948.
13 J. Li, S. Yao, Y. Lei, J. Yu and W. Zhang, *Int. J. Hydrogen Energy*, 2025, **102**, 260–273.
14 M. A. Abdul Rashid, A. M. Ithnin, W. J. Yahya, W. N. Izzati Wan Mahdi, N. A. Mazlan, A. A. Zulmajdi, D. A. Sugeng and K. Eiji, *Fuel*, 2025, **392**, 134873.
15 S. Osman, M. Gülüm and A. Stefaniu, *Int. J. Thermophys.*, 2025, **46**, 20.
16 Y. Hua, X. Xiang, D. Gao, L. Qiu and Y. Zhang, *Energy*, 2025, **323**, 135843.
17 B. Rajesh Kumar and S. Saravanan, *Renewable Sustainable Energy Rev.*, 2016, **60**, 84–115.
18 V. Edwin Geo, D. Jesu Godwin, S. Thiyagarajan, C. G. Saravanan and F. Aloui, *Fuel*, 2019, **256**, 115806.
19 Y. Zhang, S. Gao, Z. Zhang, W. Li, T. Yuan, D. Tan, L. Duan and G. Yang, *Fuel*, 2023, **335**, 127011.
20 J. P. Gujar and B. Modhera, *Int. J. Hydrogen Energy*, 2025, **144**, 220–238.
21 M. Sajdak, A. J. Majewski, S. Sobek, G. Gałko and M. Ouadi, *Waste Manage.*, 2025, **194**, 258–269.
22 Z. Zou, A. Wang, T. Zhang, Y. Cong and N. Li, *J. Energy Chem.*, 2025, **108**, 101–108.
23 E. Canales, S. C. Hower, D. P. Li, A. Tambe, D. Rothamer and G. W. Huber, *Sustainable Energy Fuels*, 2024, **8**, 3036–3047.
24 Z. Mehrabi, A. Taheri-Kafrani, A. Razmjou, D. Cai and H. Amiri, *Bioresour. Technol.*, 2025, **419**, 132094.
25 Z. Zhou, H. Ding, C. Shi, S. Peng, B. Zhu, X. An and H. Li, *Bioresour. Technol.*, 2025, **419**, 132035.
26 L. Zhu, H. Zhong, Z. Chen, M. Wu and K. Cheng, *Renewable Sustainable Energy Rev.*, 2025, **215**, 115637.
27 R. Purbia, S. Y. Choi, C. H. Woo, J. Jeon, C. Lim, D. K. Lee, J. Y. Choi, H.-S. Oh and J. M. Baik, *Appl. Catal. B: Environ. Energy*, 2024, **345**, 123694.
28 A. Singh, S. Barman, F. A. Rahimi, A. Dey, R. Jena, R. Kumar, N. Mathew, D. Bhattacharyya and T. K. Maji, *Energy Environ. Sci.*, 2024, **17**, 2315–2325.
29 R. E. Vos, K. E. Kolmeijer, T. S. Jacobs, W. van der Stam, B. M. Weckhuysen and M. T. M. Koper, *ACS Catal.*, 2023, **13**, 8080–8091.
30 H. Xu, D. Rebollar, H. He, L. Chong, Y. Liu, C. Liu, C.-J. Sun, T. Li, J. V. Muntean, R. E. Winans, D.-J. Liu and T. Xu, *Nat. Energy*, 2020, **5**, 623–632.
31 A. Dutta, I. Z. Montiel, R. Erni, K. Kiran, M. Rahaman, J. Drnec and P. Broekmann, *Nano Energy*, 2020, **68**, 104331.

32 W. Ma, S. Xie, T. Liu, Q. Fan, J. Ye, F. Sun, Z. Jiang, Q. Zhang, J. Cheng and Y. Wang, *Nat. Catal.*, 2020, **3**, 478–487.
33 S. Nitopi, E. Bertheussen, S. B. Scott, X. Liu, A. K. Engstfeld, S. Horch, B. Seger, I. E. L. Stephens, K. Chan, C. Hahn, J. K. Nørskov, T. F. Jaramillo and I. Chorkendorff, *Chem. Rev.*, 2019, **119**, 7610–7672.
34 Y. He, F. H. Müller, R. Palkovits, F. Zeng and C. Mebrahtu, *Appl. Catal. B: Environ. Energy*, 2024, **345**, 123663.
35 Y. Sheng, M. V. Polynski, M. K. Eswaran, B. Zhang, A. M. H. Lim, L. Zhang, J. Jiang, W. Liu and S. M. Kozlov, *Appl. Catal., B*, 2024, **343**, 123550.
36 D. Xu, Y. Wang, M. Ding, X. Hong, G. Liu and S. C. E. Tsang, *Chem*, 2021, **7**, 849–881.
37 S. De, A. Dokania, A. Ramirez and J. Gascon, *ACS Catal.*, 2020, **10**, 14147–14185.
38 F. Zeng, C. Mebrahtu, X. Xi, L. Liao, J. Ren, J. Xie, H. J. Heeres and R. Palkovits, *Appl. Catal., B*, 2021, **291**, 120073.
39 T. V. Ramachandra and D. Hebbale, *Renewable Sustainable Energy Rev.*, 2020, **117**, 109479.
40 W.-C. Wang and L. Tao, *Renewable Sustainable Energy Rev.*, 2016, **53**, 801–822.
41 C. Urban, J. Xu, H. Sträuber, T. R. dos Santos Dantas, J. Mühlenberg, C. Härtig, L. T. Angenent and F. Harnisch, *Energy Environ. Sci.*, 2017, **10**, 2231–2244.
42 O. Cavalett and F. Cherubini, *Nat. Sustainability*, 2018, **1**, 799–807.
43 M. Wang, R. Dewil, K. Maniatis, J. Wheeldon, T. Tan, J. Baeyens and Y. Fang, *Prog. Energy Combust. Sci.*, 2019, **74**, 31–49.
44 E. D. Larson, T. G. Kreutz, C. Greig, R. H. Williams, T. Rooney, E. Gray, C. Elsido, E. Martelli and J. C. Meerman, *Appl. Energy*, 2020, **260**, 114209.
45 K. S. Ng, D. Farooq and A. Yang, *Renewable Sustainable Energy Rev.*, 2021, **150**, 111502.
46 R. G. Grim, D. Ravikumar, E. C. D. Tan, Z. Huang, J. R. Ferrell, M. Resch, Z. Li, C. Mevawala, S. D. Phillips, L. Snowden-Swan, L. Tao and J. A. Schaidle, *Energy Environ. Sci.*, 2022, **15**, 4798–4812.
47 S. Xie, Z. Li, S. Luo and W. Zhang, *Renewable Sustainable Energy Rev.*, 2024, **192**, 114240.
48 A. E. Mansy, S. Daniel, C. K. Fonzeu Monguen, H. Wang, A. I. Osman and Z.-Y. Tian, *Environ. Chem. Lett.*, 2025, **23**, 419–461.
49 J. Zhang, M. S. Webber, Y. Pu, Z. Li, X. Meng, M. L. Stone, B. Wei, X. Wang, S. Yuan, B. Klein, B. Seemala, C. E. Wyman, K. K. Ramasamy, M. Thorson, M. H. Langholtz, J. S. Heyne, A. Koishybay, S. Adhikari, S. Cao, A. D. Sutton, G. A. Tuskan, Y. Román-Leshkov, A. J. Ragauskas, T. Ling and B. H. Davison, *Green Energy Environ.*, 2025, **10**, 1210–1234.
50 Q. Wei, Z. Luo, H. Sun, Q. Qian, J. Shi, C. Song and E. R. Naranov, *Energy*, 2025, **329**, 136736.
51 M. Uyttebroek, W. Van Hecke and K. Vanbroekhoven, *Catal. Today*, 2015, **239**, 7–10.
52 C. Yang, R. Mu, G. Wang, J. Song, H. Tian, Z.-J. Zhao and J. Gong, *Chem. Sci.*, 2019, **10**, 3161–3167.
53 M. R. Gogate and R. J. Davis, *Catal. Commun.*, 2010, **11**, 901–906.
54 H. Guo, S. Li, F. Peng, H. Zhang, L. Xiong, C. Huang, C. Wang and X. Chen, *Catal. Lett.*, 2015, **145**, 620–630.
55 B. An, Z. Li, Y. Song, J. Zhang, L. Zeng, C. Wang and W. Lin, *Nat. Catal.*, 2019, **2**, 709–717.
56 Y. Chen, S. Choi and L. T. Thompson, *J. Catal.*, 2016, **343**, 147–156.
57 D. L. S. Nieskens, D. Ferrari, Y. Liu and R. Kolonko, *Catal. Commun.*, 2011, **14**, 111–113.
58 L. Wang, S. He, L. Wang, Y. Lei, X. Meng and F.-S. Xiao, *ACS Catal.*, 2019, **9**, 11335–11340.
59 J.-n. Zheng, K. An, J.-m. Wang, J. Li and Y. Liu, *J. Fuel Chem. Technol.*, 2019, **47**, 697–708.
60 S. Zhang, X. Liu, Z. Shao, H. Wang and Y. Sun, *J. Catal.*, 2020, **382**, 86–96.
61 H. Du, M. Jiang, M. Zhao, X. Ma, Z. Xu and Z. Zhao, *Int. J. Hydrogen Energy*, 2022, **47**, 4559–4567.
62 S. M. Ghoreishian, K. Shariati, Y. S. Huh and J. Lauterbach, *Chem. Eng. J.*, 2023, **467**, 143533.
63 F. Papa, A. Vasile and G. Dobrescu, *Catalysts*, 2022, **12**, 1637.
64 C. Yang and Z. Y. Meng, *J. Catal.*, 1993, **142**, 37–44.
65 J. Gu, W. Gong, Q. Zhang, R. Long, J. Ma, X. Wang, J. Li, J. Li, Y. Fan, X. Zheng, S. Qiu, T. Wang and Y. Xiong, *Nat. Commun.*, 2023, **14**, 7935.
66 N. M. Eagan, M. D. Kumbhalkar, J. S. Buchanan, J. A. Dumesic and G. W. Huber, *Nat. Rev. Chem.*, 2019, **3**, 223–249.
67 K. Koda, T. Matsu-ura, Y. Obora and Y. Ishii, *Chem. Lett.*, 2009, **38**, 838–839.
68 G. Xu, T. Lammens, Q. Liu, X. Wang, L. Dong, A. Caiazzo, N. Ashraf, J. Guan and X. Mu, *Green Chem.*, 2014, **16**, 3971–3977.
69 S. Chakraborty, P. E. Piszel, C. E. Hayes, R. T. Baker and W. D. Jones, *J. Am. Chem. Soc.*, 2015, **137**, 14264–14267.
70 G. R. M. Dowson, M. F. Haddow, J. Lee, R. L. Wingad and D. F. Wass, *Angew. Chem., Int. Ed.*, 2013, **52**, 9005–9008.
71 R. L. Wingad, P. J. Gates, S. T. G. Street and D. F. Wass, *ACS Catal.*, 2015, **5**, 5822–5826.
72 T. A. DiBenedetto and W. D. Jones, *Organometallics*, 2021, **40**, 1884–1888.
73 K. N. T. Tseng, S. Lin, J. W. Kampf and N. K. Szymczak, *Chem. Commun.*, 2016, **52**, 2901–2904.
74 Y. Xie, Y. Ben-David, L. J. W. Shimon and D. Milstein, *J. Am. Chem. Soc.*, 2016, **138**, 9077–9080.
75 B. M. Farris, A. M. Davies, C. R. J. Stephenson and N. K. Szymczak, *ACS Catal.*, 2024, **14**, 8456–8462.
76 S. Fu, Z. Shao, Y. Wang and Q. Liu, *J. Am. Chem. Soc.*, 2017, **139**, 11941–11948.
77 N. V. Kulkarni, W. W. Brennessel and W. D. Jones, *ACS Catal.*, 2018, **8**, 997–1002.
78 M. Roca Jungfer, J. L. Schwarz, F. Rominger, T. Oeser, R. Paciello, A. S. K. Hashmi and T. Schaub, *ChemCatChem*, 2024, **16**, e202301588.

79 Y. Hatsukawa, T. Osawa, M. Oshima, Y. Toh, A. Kimura, M. Koizumi and K. Furutaka, *J. Radioanal. Nucl. Chem.*, 2012, **291**, 143–145.
80 M. Laiche, S. Hinaje, Y. Drissi, D. Yaagoub, M. El Fartati, Y. Ouahzizi and A. Laksir, *Heliyon*, 2025, **11**, e42650.
81 Z. Lin, L. Liu, E. Lian, W. Zhao and X. Jiang, *Sci. Total Environ.*, 2024, **928**, 172493.
82 F. D. Fenner and B. J. Presley, *Nature*, 1984, **312**, 260–262.
83 H. U. Sverdrup, K. V. Ragnarsdottir and D. Koca, *J. Cleaner Prod.*, 2017, **140**, 359–372.
84 H. W. Lakin, C. E. Thompson and D. F. Davidson, *Science*, 1963, **142**, 1568–1569.
85 B. R. Bolton, J. Ostwald and M. Monzier, *Nature*, 1986, **320**, 518–520.
86 R. A. Buchanan and F. E. Harrison, *Alzheimer's Dementia*, 2024, **20**, e093434.
87 B. Agrahari, K. Chaudhary, S. Dewan, H. Sonker, A. S.V, N. Awasthi, H. Makari, S. Sinharay and R. G. Singh, *Small*, 2025, 2503986.
88 S. Zhang, M. Shao, Y. Wu, Y.-R. Gao, F. Ma, J. Jiang, C. Chen, Z.-Y. Wang, J. W. Y. Lam, X.-L. Xu, C. Yang, J. Du, Z. Zhao and B. Z. Tang, *Aggregate*, 2025, **6**, e710.
89 X. Deng, Y. Guo, X. Jin, H. Si, K. Dai, M. Deng, J. He, C. Hao and W. Yao, *Neurotoxicology*, 2024, **102**, 1–11.
90 S. B. Kavukcu, H. K. Ensarioğlu, H. Karabıyık, H. S. Vatansever and H. Türkmen, *ACS Omega*, 2023, **8**, 37549–37563.
91 P. A. Kots, A. V. Zabilska, Y. V. Grigor'ev and I. I. Ivanova, *Pet. Chem.*, 2019, **59**, 925–934.
92 B. Lu, S. Ma, S. Liang, Z. Wang, Y. Liu, S. Mao, H. Ban, L. Wang and Y. Wang, *ACS Catal.*, 2023, **13**, 4866–4872.
93 Z. Liu, J. Liao, Y. Gong, J. Song and T. Wang, *Energy Convers. Manage.*, 2024, **299**, 117833.
94 H. Liu, T. Zheng, T. Hui, R. Zhang, X. Meng, W. Zhu, H. Liu and Z. Liu, *Chem. Eng. J.*, 2024, **481**, 148397.
95 Z. Liu, K. Wang, Y. Pang, C. Xiao, X. Wu, J. Song and T. Wang, *Fuel*, 2024, **371**, 131852.
96 Z. Liu, Y. Gong, T. Jiang, C. Xiao, Y. Pang, B. Chen, J. Song and T. Wang, *Energy*, 2025, **318**, 134866.
97 L. N. Stepanova, O. B. Belskaya, A. V. Vasilevich, T. I. Gulyaeva, N. N. Leont'eva, A. N. Serkova, A. N. Salanov and V. A. Likholobov, *Catal. Today*, 2020, **357**, 638–645.
98 S.-B. Lee, E.-H. Ko, J. Y. Park and J.-M. Oh, *Nanomaterials*, 2021, **11**, 1153.
99 Z.-H. Zhang, Z. Sun and T.-Q. Yuan, *Trans. Tianjin Univ.*, 2022, **28**, 89–111.
100 M. F. Guo, M. J. Gray, H. Job, C. Alvarez-Vasco, S. Subramaniam, X. Zhang, L. Kovarik, V. Murugesan, S. Phillips and K. K. Ramasamy, *Green Chem.*, 2021, **23**, 8030–8039.
101 J. I. Di Cosimo, C. R. Apesteguía, M. J. L. Ginés and E. Iglesia, *J. Catal.*, 2000, **190**, 261–275.
102 J. Zhang, K. Shi, Z. An, Y. Zhu, X. Shu, H. Song, X. Xiang and J. He, *Ind. Eng. Chem. Res.*, 2020, **59**, 3342–3350.
103 B. Yuan, J. Zhang, Z. An, Y. Zhu, X. Shu, H. Song, X. Xiang, W. Wang, Y. Jing, L. Zheng and J. He, *Appl. Catal., B*, 2022, **309**, 121271.
104 M. Rechi Siqueira, O. Micali Perrone, G. Metzker, D. C. de Oliveira Lisboa, J. C. Thoméo and M. Boscolo, *Mol. Catal.*, 2019, **476**, 110516.
105 W.-L. Lv, L. He, W.-C. Li, B.-C. Zhou, S.-P. Lv and A.-H. Lu, *Green Chem.*, 2023, **25**, 2653–2662.
106 Z. Wang, M. Yin, J. Pang, X. Li, Y. Xing, Y. Su, S. Liu, X. Liu, P. Wu, M. Zheng and T. Zhang, *J. Energy Chem.*, 2022, **72**, 306–317.
107 T. A. DiBenedetto and W. D. Jones, *Organometallics*, 2021, **40**, 1884–1888.
108 W. Liu, J. Sun, X. Zhang and M. Wei, *Ind. Eng. Chem. Res.*, 2018, **57**, 15606–15612.
109 C. R. Ho, S. Shylesh and A. T. Bell, *ACS Catal.*, 2016, **6**, 939–948.
110 L. Silvester, J.-F. Lamonier, C. Lamonier, M. Capron, R.-N. Vannier, A.-S. Mamede and F. Dumeignil, *ChemCatChem*, 2017, **9**, 2250–2261.
111 H. Brasil, A. F. B. Bittencourt, K. C. E. S. Yokoo, P. d. C. D. Mendes, L. G. Verga, K. F. Andriani, R. Landers, J. L. F. d. Silva and G. P. Valença, *J. Catal.*, 2021, 802–813, DOI: **10.1016/j.jcat.2021.08.050**.
112 T. Tsuchida, T. Yoshioka, S. Sakuma, T. Takeguchi and W. Ueda, *Ind. Eng. Chem. Res.*, 2008, **47**, 1443–1452.
113 S. Ogo, A. Onda and K. Yanagisawa, *Appl. Catal., A*, 2011, **402**, 188–195.
114 B.-C. Zhou, W.-C. Li, W.-L. Lv, S.-Y. Xiang, X.-Q. Gao and A.-H. Lu, *ACS Catal.*, 2022, **12**, 12045–12054.
115 M. V. Landau, T. Hos, R. Vidruk Nehemya, G. Nomikos and M. Herskowitz, *Catalysts*, 2021, **11**, 498.
116 M. Xue, B. Yang, C. Xia and G. Zhu, *ACS Sustainable Chem. Eng.*, 2022, **10**, 3466–3476.
117 M. Xue, Z. Jin, B. Yang, C. Xia and G. Zhu, *ACS Catal.*, 2024, **14**, 12654–12663.
118 D. Chen, J. Liu, B. Liu, Y. Qin, X. Lin and X. Qiu, *Adv. Mater.*, 2025, **37**, 2501113.
119 X. Lin, D. Chen, X. Qiu, B. Liu, J. Liu, X. Wang, S. Sun and Y. Qin, *Adv. Energy Mater.*, 2024, **14**, 2303442.
120 J. Liu, X. Qiu, S. Sun, B. Liu, Y. Tian, Y. Qin and X. Lin, *Green Chem.*, 2024, **26**, 8020–8029.
121 B. Liu, Y. Qi, X. Qiu, H. Zou, X. Lin and Y. Qin, *Adv. Funct. Mater.*, 2025, **35**, 2421552.
122 Z. Wei, X. Wang, X. Lin and X. Qiu, *Chin. J. Chem. Eng.*, 2025, **79**, 241–251.
123 X. Lin, P. Wang, R. Hong, X. Zhu, Y. Liu, X. Pan, X. Qiu and Y. Qin, *Adv. Funct. Mater.*, 2022, **32**, 2209262.
124 Y. She, X. Li, Y. Zheng, D. Chen, X. Rui, X. Lin and Y. Qin, *Energy Environ. Mater.*, 2024, **7**, e12538.
125 T. J. Szalaty, Ł. Klapiszewski and T. Jesionowski, *J. Mol. Liq.*, 2020, **301**, 112417.
126 Z. Yang, H. Guo, G. Yan, X. Li, Z. Wang, Y. Guo, X. Wang, Y. Wu and J. Wang, *ACS Sustainable Chem. Eng.*, 2020, **8**, 11522–11531.

127 M. Mennani, M. Kasbaji, A. Ait Benhamou, A. Boussetta, A. A. Mekkaoui, N. Grimi and A. Moubarik, *Green Chem.*, 2023, **25**, 2896–2929.
128 X. Lin, J. Liu, X. Qiu, B. Liu, X. Wang, L. Chen and Y. Qin, *Angew. Chem., Int. Ed.*, 2023, **62**, e202306333.
129 X. Lin, J. Liu, L. Wu, L. Chen, Y. Qi, Z. Qiu, S. Sun, H. Dong, X. Qiu and Y. Qin, *AIChE J.*, 2022, **68**, e17785.
130 X. Liu, J. Fu, Y. Tang, R. L. Smith Jr and X. Qi, *Chem. Eng. J.*, 2021, **406**, 126748.
131 X. Wang, M. Qiu, R. L. Smith Jr., J. Yang, F. Shen and X. Qi, *ACS Sustainable Chem. Eng.*, 2020, **8**, 18157–18166.
132 X. Wang, X. Liu, R. L. Smith, Y. Liang and X. Qi, *Green Chem.*, 2021, **23**, 8632–8642.
133 I. Nezam, J. Zak and D. J. Miller, *Ind. Eng. Chem. Res.*, 2020, **59**, 13906–13915.
134 S. Pithakratanayothin, R. Tongsri, T. Chaisuwan and S. Wongkasemjit, *Catal. Sci. Technol.*, 2017, **7**, 5413–5421.
135 X. Fei, Q. Xu, L. Xue, X. Zhong, Z. Zhang, K. Liu, X. Lin, T. Wang, Y. Qin and X. Qiu, *Ind. Eng. Chem. Res.*, 2021, **60**, 17959–17969.
136 X. Lin, X. Fei, D. Chen, Y. Qi, Q. Xu, Y. Liu, Q. Zhang, S. Li, T. Wang, Y. Qin and X. Qiu, *ACS Catal.*, 2022, **12**, 11573–11585.
137 Q. Xu, X. Fei, X. Qiu, X. Wang, T. Wang, X. Lin, S. Li and Y. Qin, *Chem. Eng. J.*, 2024, **489**, 151092.
138 B. Chen, X. Zheng, J. Gu, S. Qiu, J. Song, X. Wu, H. Dong, Q. Zhang and T. Wang, *Appl. Catal., B*, 2023, **321**, 122048.
139 Q. Zhong, J. Liao, Q. Zhang, S. Qiu, Q. Meng, X. Wu and T. Wang, *Fuel*, 2022, **324**, 124507.
140 J. Liao, Z. Liu, Y. Ling, Q. Zhang, S. Qiu, J. Gu, J. Li, H. Dong, J. Song and T. Wang, *Chem. Eng. J.*, 2023, **461**, 141888.
141 X. Wu, G. Zou, J. Hou, X. Liu, M. Li, X. Cai, Q. Zhang, Y. Pi, Q. Meng and T. Wang, *Chem. Eng. Sci.*, 2024, **292**, 120013.
142 X. Cai, X. Li, M. Dang, H. Huang, A. Liu, Q. Zhang, Y. Pi, Q. Meng, X. Wu and T. Wang, *Fuel*, 2023, **335**, 126971.
143 X. Zheng, B. Chen, J. Gu, S. Qiu, X. Wu, Q. Zhang and T. Wang, *Green Chem.*, 2024, **26**, 3507–3516.
144 J. Gu, K. Mao, Q. Zhang, B. Chen, H. Dong, S. Qiu, Q. Meng, Y. Xiong, J. Song and T. Wang, *Chem. Eng. J.*, 2023, **453**, 139583.
145 L. Yuan, M. Zhang, G. Fan and F. Li, *Appl. Catal., B*, 2024, **343**, 123488.
146 J. Pang, M. Zheng, Z. Wang, S. Liu, X. Li, X. Li, J. Wang and T. Zhang, *Chin. J. Catal.*, 2020, **41**, 672–678.
147 D. Jiang, X. Wu, J. Mao, J. Ni and X. Li, *Chem. Commun.*, 2016, **52**, 13749–13752.
148 Z. Wang, J. Pang, L. Song, X. Li, Q. Yuan, X. Li, S. Liu and M. Zheng, *Ind. Eng. Chem. Res.*, 2020, **59**, 22057–22067.
149 Z. Wang, M. Yin, J. Pang, P. Wu, L. Song, X. Li and M. Zheng, *Ind. Eng. Chem. Res.*, 2023, **62**, 2594–2604.
150 Z. Cheng, Y. Wang, D. Jin, J. Liu, W. Wang, Y. Gu, W. Ni, Z. Feng and M. Wu, *Catal. Today*, 2023, **410**, 164–174.
151 Y. Ma, C. Weimer, N. Yang, L. Zhang, T. Staedler and X. Jiang, *Mater. Today Commun.*, 2015, **2**, e55–e61.
152 Y.-E. Miao, F. Li, H. Lu, J. Yan, Y. Huang and T. Liu, *Compos. Commun.*, 2016, **1**, 15–19.
153 K. Chhetri, S. Subedi, A. Muthurasu, T. H. Ko, B. Dahal and H. Y. Kim, *J. Energy Storage*, 2022, **46**, 103927.
154 C. Yang, Z.-D. Yang, R. Zhang and G. Zhang, *Chem. Phys.*, 2019, **517**, 104–112.
155 D. Kobina Sam, E. Kobina Sam and X. Lv, *ChemElectroChem*, 2020, **7**, 3695–3712.
156 D. K. Sam, E. K. Sam, A. Durairaj, X. Lv, Z. Zhou and J. Liu, *Carbohydr. Res.*, 2020, **491**, 107986.
157 G. Yang, L. Li, W. B. Lee and M. C. Ng, *Sci. Technol. Adv. Mater.*, 2018, **19**, 613–648.
158 T. Yang, H. Lin, X. Zheng, K. P. Loh and B. Jia, *J. Mater. Chem. A*, 2017, **5**, 16537–16558.
159 H.-L. Gao, Y.-B. Zhu, L.-B. Mao, F.-C. Wang, X.-S. Luo, Y.-Y. Liu, Y. Lu, Z. Pan, J. Ge, W. Shen, Y.-R. Zheng, L. Xu, L.-J. Wang, W.-H. Xu, H.-A. Wu and S.-H. Yu, *Nat. Commun.*, 2016, **7**, 12920.
160 M. B. Bryning, D. E. Milkie, M. F. Islam, L. A. Hough, J. M. Kikkawa and A. G. Yodh, *Adv. Mater.*, 2007, **19**, 661–664.
161 K. Huo, Y. Sun, H. Jiang, S. Lin, H. Fang, Z. Cheng, S. Cao, L. Li, Y. Wang and M. Wu, *Molecules*, 2024, **29**, 4642.
162 L. Sun, Y. Gong, D. Li and C. Pan, *Green Chem.*, 2022, **24**, 3864–3894.
163 J. S. Bulmer, A. Kaniyoor and J. A. Elliott, *Adv. Mater.*, 2021, **33**, 2008432.
164 D. Kobina Sam, H. Li, Y.-T. Xu and Y. Cao, *J. Ind. Eng. Chem.*, 2024, **135**, 17–42.
165 M. Hartmann and W. Schwieger, *Chem. Soc. Rev.*, 2016, **45**, 3311–3312.
166 X.-Y. Yang, L.-H. Chen, Y. Li, J. C. Rooke, C. Sanchez and B.-L. Su, *Chem. Soc. Rev.*, 2017, **46**, 481–558.
167 X. Zhou, Y. Liu, C. Du, Y. Ren, T. Mu, P. Zuo, G. Yin, Y. Ma, X. Cheng and Y. Gao, *J. Power Sources*, 2018, **381**, 156–163.
168 X. Jiang, Y. Chen, X. Meng, W. Cao, C. Liu, Q. Huang, N. Naik, V. Murugadoss, M. Huang and Z. Guo, *Carbon*, 2022, **191**, 448–470.
169 K. P. Shejale, Y. Krishnan, R. K. Dharman, Y. Uk Jeong and S. Yeol Kim, *Mater. Des.*, 2023, **227**, 111782.
170 D. Xu, Q. Ding, J. Li, H. Chen, Y. Pan and J. Liu, *Inorg. Chem. Commun.*, 2020, **119**, 108141.
171 H. Ye, S. Xin, Y.-X. Yin and Y.-G. Guo, *Adv. Energy Mater.*, 2017, **7**, 1700530.
172 Q. Luo, H. Zheng, Y. Hu, H. Zhuo, Z. Chen, X. Peng and L. Zhong, *Ind. Eng. Chem. Res.*, 2019, **58**, 17768–17775.
173 H. Guo, Z. Guo, G. Xue, H. Wang, J. Gong, K. Chu, J. Qin, Y. Guan, H. Dong, Y. Chen, Y.-E. Miao, C. Zhang, H. Liu, T. Liu, J. Hofkens and F. Lai, *Adv. Mater.*, 2025, 2500224.
174 Z. Chen, M. Qin, Y. Xie, Y. Guo, C. Dong, C. Wang and Y.-H. Qin, *J. Hazard. Mater.*, 2025, **488**, 137327.
175 Y. Liu, Z. Shao, Y. Wang, L. Xu, Z. Yu and Q. Liu, *ChemSusChem*, 2019, **12**, 3069–3072.

176 X. Wu, X. Cai, Q. Zhang, P. Bi, Q. Meng, Y. Pi and T. Wang, *ACS Sustainable Chem. Eng.*, 2021, **9**, 11269–11279.
177 D. He, J. Zhou and K. Fang, *Mol. Catal.*, 2025, **580**, 115079.
178 O. V. Zikrata, O. V. Larina, K. V. Valihura, P. I. Kyriienko, D. Y. Balakin, I. Khalakhan, K. Veltruská, A. Krajnc, G. Mali, S. O. Soloviev and S. M. Orlyk, *ACS Sustainable Chem. Eng.*, 2021, **9**, 17289–17300.
179 J. Hou, G. Zou, X. Liu, M. Li, P. Yang, X. Zhang, Y. Chen, Q. Zhang, X. Wu and T. Wang, *Ind. Eng. Chem. Res.*, 2025, **64**, 10667–10677.
180 S. Meng, Z. Cui, Q. Chen, H. Zhang, S. Li, E. C. Neyts, E. Vlasov, K. Jenkinson, S. Bals, D. Yang, M. Liu, Y. Liu, A. Bogaerts, A.-H. Lu and Y. Yi, *ACS Catal.*, 2025, **15**, 3236–3246.
181 J. Li, R. Yang, S. Xu, C. Zhou, Y. Xiao, C. Hu and D. C. W. Tsang, *Appl. Catal., B*, 2022, **317**, 121785.
182 B. M. Trost, *Science*, 1991, **254**, 1471–1477.
183 R. A. Sheldon, *Green Chem.*, 2007, **9**, 1273–1283.
184 A. Antenucci and S. Dughera, *Catalysts*, 2023, **13**, 102.
185 M. Meli, Z. Wang, S. Sterlepper, M. Picerno and S. Pischinger, *Appl. Energy*, 2025, **392**, 125893.
186 Z. Li, Y. Wang, H. Liu, Y. Feng, X. Du, Z. Xie, J. Zhou, Y. Liu, Y. Song, F. Wang, M. Sui, Y. Lu, F. Fang and D. Sun, *Nat. Mater.*, 2025, **24**, 424–432.
187 F. Zhang, B. Zu, B. Wang, Z. Qin, J. Yao, Z. Wang, L. Fan and K. Jiao, *Joule*, 2025, **9**, 101853.
188 J. Han, K. Park, S. Tan, Y. Vaynzof, J. Xue, E. W.-G. Diau, M. G. Bawendi, J.-W. Lee and I. Jeon, *Nat. Rev. Methods Primers*, 2025, **5**, 3.
189 Q. Liu, X. Wen, H. Peng and Q. Cao, *J. Cleaner Prod.*, 2023, **423**, 138635.
190 A. Kerschbaum, L. Trentmann, A. Hanel, S. Fendt and H. Spliethoff, *Renewable Sustainable Energy Rev.*, 2025, **215**, 115559.
191 K. I. Kiouranakis, P. de Vos, K. Zoumpourlos, A. Coraddu and R. Geertsma, *Renewable Sustainable Energy Rev.*, 2025, **214**, 115529.
192 A. Lu and Y. Zhu, *Energy*, 2025, **322**, 135715.
193 R. Patiño-Camino, A. Cova-Bonillo, F. Villanueva, Á. Ramos, V. M. Domínguez, J. Rodríguez-Fernández and J. J. Hernández, *Fuel*, 2025, **392**, 134916.
194 H. Chi, Z. Liang, S. Kuang, Y. Jin, M. Li, T. Yan, J. Lin, S. Wang, S. Zhang and X. Ma, *Nat. Commun.*, 2025, **16**, 979.
195 R. Fang, J. Kang, F. Wang, X. Zhao and Y. Li, *ACS Catal.*, 2025, **15**, 4403–4414.
196 L. Ge, M. M. Ali, A. I. Osman, A. M. Elgarahy, M. Samer, Y. Xu and Z. Liu, *Renewable Sustainable Energy Rev.*, 2025, **217**, 115726.
197 D. Sun, Y. Zhang, Y. Zhou, Y. Nie, L. Ban, D. Wu, S. Yang, H. Zhang, C. Li and K. Zhang, *Adv. Energy Mater.*, 2025, 2406098.
198 F. Xie, X. Meng, Y. Liu, L. Han, Y. Gong, C. Zhang, X. Li, Y. Zhou and H. Dou, *Fuel Process. Technol.*, 2025, **269**, 108190.
199 P. Ventin, M. Lapuerta, F. A. Torres, E. A. Torres and J. J. Hernández, *Fuel*, 2025, **390**, 134730.
200 H. Feng, X. Chen, L. Sun, R. Ma, X. Zhang, L. Zhu and C. Yang, *Energy*, 2023, **282**, 128792.
201 Y.-C. Hu, Y. Zhao, N. Li and J.-P. Cao, *J. Energy Chem.*, 2024, **95**, 712–722.
202 K. Lakzian, H.-J. Liaw, E. Lakzian and V. Gerbaud, *Prog. Energy Combust. Sci.*, 2025, **108**, 101222.
203 P. J. Ansell, *Prog. Aeronaut. Sci.*, 2023, **141**, 100919.
204 E. Oğur, A. Koç, H. Yağlı, Ö. Köse and Y. Koç, *Energy*, 2025, **316**, 134426.
205 K. Kim, P. Wiersema, J. Ir Ryu, W. Lee, K. Min, E. Mayhew, J. Temme, C.-B. M. Kweon and T. Lee, *Fuel*, 2024, **368**, 131630.
206 L. H. Nogueira Marinho, F. V. Aragão, D. M. de Genaro Chiroli, F. C. Zola and S. M. Tebcherani, *Fuel*, 2025, **402**, 135924.
207 G. Inc, *Focus Catal.*, 2021, **2021**, 6.
208 G. Inc, *Focus Catal.*, 2022, **2022**, 5.
209 Y. Zhang, W. Dong, R. Xu, G. P. Smith and H. Wang, *Combust. Flame*, 2024, **259**, 113168.
210 C. Sheridan, *Nat. Biotechnol.*, 2024, **42**, 1628–1628.
211 Z. Xu, Y. Fan, Y. Zheng, S. Ding, M. Zhu, G. Li, M. Wang, Z. Yu, Y. Song, L. Chang and L. Chen, *Environ. Pollut.*, 2025, **368**, 125661.
212 K. Jeske, T. Rösler, M. Belleflamme, T. Rodenas, N. Fischer, M. Claeys, W. Leitner, A. J. Vorholt and G. Prieto, *Angew. Chem., Int. Ed.*, 2022, **61**, e202201004.
213 L. Yuan, H. Li, Z. Zhang, G. Fan and F. Li, *Ind. Eng. Chem. Res.*, 2025, **64**, 4771–4783.
214 Q. Shi, Y.-Q. Zhu, X. Liu, B.-J. Yuan, W. Tang, X. Wang, R.-P. Li and H. Duan, *J. Am. Chem. Soc.*, 2025, **147**, 14004–14014.
215 H. Ryu, M. Sung, H. Baek, S. Lee, B. Seo, K. Shin, M. Noh, J. Jang, J. Bae Lee and J. Woong Kim, *Chem. Eng. J.*, 2024, **486**, 149701.
216 K. Aramaki, Y. Matsuura, K. Kawahara, D. Matsutomo and Y. Konno, *J. Oleo Sci.*, 2021, **70**, 67–76.
217 H. Song, S. Lei, W. Fang, F. Jin, M. Kang, J. Chen and H. Liu, *RSC Adv.*, 2025, **15**, 19339–19347.
218 M. Depta, S. Napiórkowski, K. Zielińska, K. Gębura, D. Niewolik and K. Jaszcz, *Materials*, 2024, **17**, 3072.
219 J. N. Nair, T. Nagadurga, V. D. Raju, H. Venu, S. Algburi, S. Kamangar, A. I. Ali Arabi, A. Razak and N. Marakala, *Case Stud. Therm. Eng.*, 2025, **67**, 105755.
220 Q. Huang, J. Li, C. Ma, N. Wang, J. Pi, Z. Zhang, K. Chang, L. Kong, Y. Yang, X. Guo, Z. Wang, J. Zhang, C. Pan, Y. Hu and Z. Liu, *Sep. Purif. Technol.*, 2025, **358**, 130252.
221 C. Fernández-Blanco, K. Sabbe, M. C. Veiga, C. Kennes and R. Ganigué, *Sep. Purif. Technol.*, 2025, **361**, 131411.
222 J. Li, X. Zhao, Y. Fan, C. Sun, Y. Hu, L. Zhang, F. Zhu and J. Han, *Chem. Eng. J. Adv.*, 2025, **23**, 100778.
223 M. Ji, Y. Chen, Y. Wang, F. Zhang, J. Li, H. Pan, Y. Zhao, Z. Zhang and L. Liu, *Tribol. Lett.*, 2024, **72**, 42.
224 Y. He, Z. Bi, Q. Zhang, S. Lu, Z. Huang, X. Zhang, X. Li and J. Dong, *Langmuir*, 2025, **41**, 5255–5267.

225 A. Sarı, A. Can, E. Çakır, N. Batan, S. Kolaylı and O. Gencel, *Mater. Chem. Phys.*, 2025, **344**, 131122.
226 V. Santhosh Reddy, S. Venkatachalapathy and P. V. R. Nanda Kishore, *Appl. Therm. Eng.*, 2024, **257**, 124138.
227 Y. Cheng, W. Guan, L. Tang, Y. Huang and W. Yang, *Colloids Surf., A*, 2024, **685**, 133319.
228 K. Naveen, T. Mahvelati-Shamsabadi, P. Sharma, S.-h. Lee, S. H. Hur, W. M. Choi, T. J. Shin and J. S. Chung, *Appl. Catal., B*, 2023, **328**, 122482.
229 Y. Wan, R. Li, J. Su, W. Yi, Y. Li, H. Chu, Z. Shen, S. Gao, X. Hai, R. Zhong and R. Zou, *Adv. Mater.*, 2025, 2504518.
230 R. Ma, D. P. Dean, J. Gao, M. Wang, Y. Liu, K. Liang, J. Wang, J. T. Miller, B. Zhou, G. Zou and J. Kou, *Appl. Catal. B: Environ. Energy*, 2024, **347**, 123798.
231 L. Kang, B. Zhu, Q. Gu, X. Duan, L. Ying, G. Qi, J. Xu, L. Li, Y. Su, Y. Xing, Y. Wang, G. Li, R. Li, Y. Gao, B. Yang, X. Y. Liu, A. Wang and T. Zhang, *Nat. Chem.*, 2025, **17**, 890–896.
232 A. Vice, E. Seger-Pera, L. Reardon and O. Kedem, *ChemCatChem*, 2025, **17**, e202401825.
233 P. Cantarero Gómez, R. Fernández de Luis, I. Oyarzabal, P. Luis Arias, M. A. Ortuño and I. Agirrezabal-Telleria, *Appl. Catal. B: Environ. Energy*, 2025, **371**, 125198.

